Prediction of response to immune checkpoint blockade in patients with metastatic colorectal cancer with microsatellite instability

T. Ratovomanana, R. Nicolle, R. Cohen, A. Diehl, A. Siret, Q. Letourneur, O. Buhard, A. Perrier, E. Guillerm, F. Coulet, et al.

Prediction of Response to Immune Checkpoint Blockade in Patients with Metastatic Colorectal Cancer with Microsatellite Instability

Journal:	*Annals of Oncology*
Manuscript ID	ANNONC-2023-0129
Article Type:	Original Article
Date Submitted by the Author:	06-Feb-2023
Complete List of Authors:	Ratovomanana, Toky; UMRS 938 - CRSA, Oncology Department Nicolle, Rémy; 2- Université Paris Cité, Centre de Recherche sur l'Inflammation, Oncology Department Cohen, Romain; Sorbonne Université, medical oncology Diehl, Aurélien; 1- Sorbonne Université, INSERM, Unité Mixte de Recherche Scientifique 938 and SIRIC CURAMUS, Oncology Department Siret, Aurélie; UMRS 938 - CRSA, Oncology Department Letourneur, Quentin; UMRS 938 - CRSA, Oncology Department Buhard, Olivier; INSERM, U938 Perrier, Alexandre; UMRS 938 - CRSA, Oncology Department Guillerm, Erell; INSERM, U938 Coulet, Florence; UMRS 938 - CRSA, Oncology Department Cervera, Pascale; UMRS 938 - CRSA, Oncology Department Benusiglio, Patrick; GH Pitié-Salpêtrière APHP, UF d'Oncogénétique; Sorbonne Université, medical oncology Labreche, Karim; UMRS 938 - CRSA, Oncology Department Colle, Raphael; Hospital Saint-Antoine, Department of Medical Oncology Collura, Ada; INSERM, U938 Despras, Emmanuelle; UMRS 938 - CRSA, Oncology Department Le Rouzic, Philippe; UMRS 938 - CRSA, Oncology Department Renaud, Florence; UMRS 938 - CRSA, Oncology Department Cros, Jerome; Hopital Bichat - Claude-Bernard, Pathology Alentorn, Agusti; Assistance Publique - Hopitaux de Paris, Service Neurologie -2 Touat, Mehdi; UMRS 938 - CRSA, Oncology Department Ayadi, Mira; Ligue Nationale Contre Le Cancer, CIT Bourgoin, Pierre; Sorbonne Université, medical oncology Prunier, Céline; UMRS 938 - CRSA, Oncology Department TOURNIGAND, Christophe; AP-HP, Henri-Mondor University Hospital,

	Department of Medical Oncology de la Fouchardière, Christelle; Hospices Civils de Lyon-Centre Anti-Cancéreux Léon-Bérard, Consortium Cancer Thyroïdien; Centre Léon Bérard, Medical Oncology tougeron, david; Poitiers university hospital, gastroenterology Jonchere, Vincent; UMRS 938 - CRSA, Oncology Department Bennouna, Jaafar; Institut de Cancerologie de l'Ouest, Oncology de Reyniès, Aurèlien; Cordeliers Research Centre, Cancer, Immune control, and Escape Flejou, Jean-François; UMRS 938 - CRSA, Oncology Department SVRCEK, Magali; INSERM U938, APHP Hôpital Saint Antoine; AP-HP, Hôpital Saint-Antoine, Pathology André, Thierry; Sorbonne Universités, Hôpital Saint Antoine, Oncologie Médicale; Sorbonne Université Duval, Alex; UMRS 938 - CRSA, Oncology Department
Keywords:	Metastatic Colorectal Cancer, Microsatellite Instability, Immune Checkpoint Inhibitors (ICI), DNA and RNA sequencing, prediction of MSI mCRC patient response to ICI, progression-free survival by iRECIST
Abstract:	Background: Mismatch repair deficient (dMMR) tumors displaying microsatellite instability (MSI) represent a paradigm for the success of immune checkpoint inhibitor (ICI)-based immunotherapy, particularly in patients with metastatic colorectal cancer (mCRC). However, a proportion of patients with dMMR/MSI mCRC exhibit resistance to ICI. Identification of tools predicting MSI mCRC patient response to ICI are required for the design of future strategies further improving this therapy. Patients and Methods: Here we combined high-throughput DNA and RNA sequencing of tumors from 116 patients with MSI mCRC treated with anti-PD-1 +/- anti-CTLA-4 of the NIPICOL phase II trial (C1, NCT03350126, discovery set) and the IMMUNOMSI prospective cohort (C2, validation set). Were clinically relevant the DNA/RNA predictors whose status was significantly associated with ICI response in both C1 and C2. Primary endpoint was iPFS (progression-free survival by iRECIST). Results: Analyses failed to validate previously suggested DNA/RNA indicators of resistance to ICI, e.g. MSISensor score, tumor mutational burden, or specific cellular and molecular tumoral contingents. By contrast, iPFS under ICI was shown in C1 and C2 to depend both on a multiplex MSI signature involving the mutations of 19 microsatellites (HRC2 = 13.1; 95% CI (2.71-63.8) ; p = 1.4x10-3) and the expression of a set of 182 RNA markers with a non-epithelial TGFB-related desmoplastic orientation (HRC2 = 4.12 ; 95% CI (1.44-11.8) ; p = 4.19x10-3). Both DNA (HRC2 = 6.05; 95% CI (1.68-21.8) ; p = 5.92x10-3) and RNA (HRC2 = 8.38 ; 95% CI (2.44-28.7) ; p = 7.22x10-4) signatures were independently predictive of iPFS. Conclusions: iPFS in patients with MSI mCRC can be predicted by simply analyzing the mutational status of DNA microsatellite-containing genes in epithelial tumor cells together with nonepithelial TGFB-related desmoplastic RNA markers. These DNA/RNA signatures are readily available to be used in clinics.

Prediction of Response to Immune Checkpoint Blockade in Patients with Metastatic Colorectal Cancer with Microsatellite Instability

Toky Ratovomanana [1€], Rémy Nicolle [2,3€], Romain Cohen [1,3,4], Aurélien Diehl [1], Aurélie Siret [1], Quentin Letourneur [1], Olivier Buhard [1], Alexandre Perrier [1,5], Erell Guillerm [1,5], Florence Coulet [1,5], Pascale Cervera [1], Patrick Benusiglio [1,5], Karim Labrèche [6], Raphaël Colle [1,3,4], Ada Collura [1], Emmanuelle Despras [1], Philippe Le Rouzic [1], Florence Renaud [1], Jérome Cros [7], Agusti Alentorn [8], Mehdi Touat [8], Mira Ayadi [9], Pierre Bourgoin [1,10], Céline Prunier [11], Christophe Tournigand [12], Christelle de la Fouchardière [13], David Tougeron [14], Vincent Jonchère [1], Jaafar Bennouna [15], Aurélien de Reynies [16], Jean-François Fléjou [1,10], Magali Svrcek [1,10], Thierry André [1,3,4], **Alex Duval [1,5 $]**

1- Sorbonne Université, INSERM, Unité Mixte de Recherche Scientifique 938 and SIRIC CURAMUS, Centre de Recherche Saint-Antoine, Equipe Instabilité des Microsatellites et Cancer, Equipe labellisée par la Ligue Nationale contre le Cancer, F-75012 Paris, France
2- Université Paris Cité, Centre de Recherche sur l'Inflammation (CRI), INSERM, U1149, CNRS, ERL 8252, F-75018 Paris, France.
3- GERCOR, Groupe Coopérateur Multidisciplinaire en Oncologie, F-75011 Paris, France.
4- Sorbonne Université, Department of Medical Oncology, AP-HP, hôpital Saint-Antoine, F-75012 Paris, France.
5- Sorbonne Université, Department of Molecular Biology and Medical Genetics, AP-HP, Hospital Pitié-Salpêtrière, F-75012 Paris, France.
6- CinBioS, MS 37 PASS Production de données en Sciences de la vie et de la Santé, INSERM, Sorbonne Université et SIRIC CURAMUS, 75013 Paris.
7- Department of Pathology, Beaujon Hospital, AP-HP, Clichy, France.
8- Service de Neurologie 2-Mazarin, Sorbonne Université, Inserm, CNRS, UMR S 1127, Institut du Cerveau, ICM, AP-HP, Hôpitaux Universitaires La Pitié Salpêtrière - Charles Foix, 47-83 boulevard de l'Hôpital, 75013, Paris, France.
9- Programme “Cartes d’Identité des Tumeurs”, Ligue Nationale Contre le Cancer, Paris, France.
10- Sorbonne Université, Department of Pathology, AP-HP, hôpital Saint-Antoine, F-75012 Paris, France.

11- Sorbonne Université, INSERM, Unité Mixte de Recherche Scientifique 938 and SIRIC CURAMUS, Centre de Recherche Saint-Antoine, Equipe Signalisation TGFB, plasticité cellulaire et Cancer, F-75012 Paris, France.
12- Department of medical Oncology, Hôpital henri Mondor, APHP, Université Paris Est Creteil, INSERM U955.
13- Department of Medical Oncology, Centre Léon Bérard, Lyon, France.
14- ProDicET, UR 24144, University of Poitiers and Hepato-Gastroenterology Department, Poitiers University Hospital, 86000 Poitiers, France.
15- Centre De Recherche En Cancérologie Et Immunologie Nantes-Angers (CRCINA), INSERM, Université d'Angers, Université De Nantes, Nantes, France.
16- Cartes d'Identité des Tumeurs Program, Ligue Nationale Contre Cancer, Paris, France.

€ Co-first Author

$ Leadership, Corresponding author

RUNNING HEAD: Prediction of Response to Immune Checkpoint Blockade in dMMR/MSI mCRC

CORRESPONDENCE: Address correspondence to: Alex Duval, Team "Microsatellite Instability and Cancer", Inserm UMRS 938, CRSA, Sorbonne University, Hôpital Saint-Antoine, Paris 75010, France. e-mail: alex.duval@inserm.fr

ACKNOWLEDGMENTS: The authors thank the patients and their families for making the study possible. The authors acknowledge the GERCOR clinical study teams, the IDEATION study group and investigators and study teams in all centers.

FUNDING: This work was supported by grants from Site de Recherche Intégré sur le Cancer (SIRIC) Cancer United Research Associating Medicine, University & Society (CURAMUS), and the Ligue Nationale Contre le Cancer. T.R was a recipient of a grant from the Region Ile-de-France (PhD Student bursary). Prof. Duval's team has the label de La Ligue contre le Cancer.

AUTHOR CONTRIBUTIONS: study concept and design: TR, RN, Adi, ADu; acquisition of data: TR, RN, RCoh, Adi, AS, QL, OB, AP, EG, FC, PC, RCol, AC, ED, PLR, FR, AA, MT, FB, MA, PB, CP, VJ, JB, AdR, JFF, MS, CT, CdlF, DT, TA, ADu; analysis and interpretation of data: TR, RN, RCoh, Adi, KL, JC, ADu; drafting of the manuscript: TR, RN, RCoh, Adi, ADu; obtained funding; ADu; technical support: TR, RN, Adi, AS, QL, OB, FC, AC, FR, PB, VJ ; study supervision: ADu.

DISCLOSURE: The authors declare no conflict of interest

ABSTRACT

Background: Mismatch repair deficient (dMMR) tumors displaying microsatellite instability (MSI) represent a paradigm for the success of immune checkpoint inhibitor (ICI)-based immunotherapy, particularly in patients with metastatic colorectal cancer (mCRC). However, a proportion of patients with dMMR/MSI mCRC exhibit resistance to ICI. Identification of tools predicting MSI mCRC patient response to ICI are required for the design of future strategies further improving this therapy.

Patients and Methods: Here we combined high-throughput DNA and RNA sequencing of tumors from 116 patients with MSI mCRC treated with anti-PD-1 +/- anti-CTLA-4 of the NIPICOL phase II trial (C1, NCT03350126, discovery set) and the IMMUNOMSI prospective cohort (C2, validation set). Were clinically relevant the DNA/RNA predictors whose status was significantly associated with ICI response in both C1 and C2. Primary endpoint was iPFS (progression-free survival by iRECIST).

Results: Analyses failed to validate previously suggested DNA/RNA indicators of resistance to ICI, e.g. MSISensor score, tumor mutational burden, or specific cellular and molecular tumoral contingents. By contrast, iPFS under ICI was shown in C1 and C2 to depend both on a multiplex MSI signature involving the mutations of 19 microsatellites (HR_{C2} = 13.1; 95% CI [2.71-63.8] ; p = $1.4x10^{-3}$) and the expression of a set of 182 RNA markers with a non-epithelial TGFB-related desmoplastic orientation (HR_{C2} = 4.12 ; 95% CI [1.44-11.8] ; p = $4.19x10^{-3}$). Both DNA (HR_{C2} = 6.05; 95% CI [1.68-21.8] ; p = $5.92x10^{-3}$) and RNA (HR_{C2} = 8.38 ; 95% CI [2.44-28.7] ; p = $7.22x10^{-4}$) signatures were independently predictive of iPFS.

Conclusions: iPFS in patients with MSI mCRC can be predicted by simply analyzing the mutational status of DNA microsatellite-containing genes in epithelial tumor cells together with nonepithelial TGFB-related desmoplastic RNA markers. These DNA/RNA signatures are readily available to be used in clinics.

Keywords: Metastatic Colorectal Cancer, Microsatellite Instability, Immune Checkpoint Inhibitors (ICI), DNA and RNA sequencing, prediction of MSI mCRC patient response to ICI, progression-free survival by iRECIST.

INTRODUCTION

Mismatch repair deficient (dMMR) tumors display a molecular phenotype characterized by the genetic instability of numerous microsatellite repeated sequences throughout the genome (Microsatellite Instability, MSI) [1-3]. MSI was first observed in inherited tumors associated with Lynch syndrome and later in a large spectrum of primary tumors, in particular sporadic colorectal cancers (CRC) (for review see [4-6]). Being highly genetically unstable, MSI cancers are highly immunogenic and generally show a strong infiltration with cytotoxic T-cell lymphocytes [4]. Recently, it was reported that MSI tumors resist this hostile immune microenvironment by overexpressing immune checkpoint (ICK)-related proteins to allow immune-escape [7]. Consistently, MSI status was shown to predict clinical benefit from ICK inhibitors (ICI) in patients with metastatic cancer including CRC (mCRC) [8, 9]. In patients pretreated with fluoropyrimidines, oxaliplatin and irinotecan prior to ICI for dMMR/MSI mCRC, the objective response rate ranges from 33% to 65% and the 1-year overall survival rate ranges from 34% to 71%. First-line pembrolizumab (anti-PD-1) has been associated with significant improvement of progression-free survival compared with standard of care chemotherapy ± cetuximab or bevacizumab [10]. However, up to 15-46% of patients with dMMR/MSI mCRC exhibit primary resistance to ICI while 5%-25% of responders develop acquired resistance to these treatments, although this estimation might increase with longer follow-up [11-14].

Several DNA and RNA-based markers predicting the efficacy of ICIs have been previously proposed in metastatic dMMR/MSI cancer settings [9, 15-21]. However, it is fair to say that these results lack independent validation, being based on the analysis of only limited series of dMMR/MSI tumor samples with heterogeneous tumor origins. At the DNA level, markers include quantitative genomic indexes measuring the level of MSI within the tumor bulk such as the MSIsensor score or the tumor mutation burden (TMB). Previous studies have considered the selection of specific somatic variants occurring in dMMR cancers due to MSI as specific predictive markers such as *BRAF*^{V600E} mutational status, *KRAS*/*NRAS* mutations, or the *B2M* truncating mutation resulting in loss of function of the resultant protein associated with the MHC class I complex [17, 20]. However, it was recently reported that B2M inactivation was unlikely to

blunt the efficacy of ICI in dMMR/MSI tumors in human [22] and using multiple murine dMMR B2m null cancer models [23], raising the question of the real impact of these somatic mutations in the MSI cancer setting. At the RNA level, it was hypothesized that the estimated abundance of specific cell populations in the tumor microenvironment could be of clinical relevance, e.g., immune cell populations such as antigen-presenting macrophages interacting with T-cells [20]. Logically, deregulated activity of some cancer-related pathways associated with antitumor immunity were also proposed, e.g., the reduced activity of *Wnt/Wingless* signaling, deregulation of the interferon gamma pathway and/or of several immune escape processes [20]. Finally, a study published by our team showed that the leading cause for association of primary resistance to ICI in mCRC was the misdiagnosis of their MSI or dMMR status [24], emphasizing that the first and foremost criteria to be validated before the prescription of ICI in metastatic dMMR/MSI cancer patients, and particularly in mCRC, is the guarantee of a quality diagnosis with appropriate methods to identify genuine dMMR/MSI.

In this study, we hypothesized that the response to ICI could be predicted by both levering on the MSI-specific mutational patterns in epithelial cells (by DNA sequencing) and by considering the modifications of the cancer stroma (by RNA sequencing) on the other hand. We addressed the issue of response to ICI based on the investigation of two independent prospective cohorts of 44 and 72 patients with dMMR/MSI mCRC, respectively the multicentric NIPICOL clinical trial (NCT03350126) [14] and the prospective ImmunoMSI cohort [25].

MATERIALS AND METHODS

Patients

The Nipicol clinical trial (C1) was conducted in accordance with the tenets of the Declaration 170 of Helsinki and Good Clinical Practice Guidelines, after approval by the ethics board, and was registered at ClinicalTrials.gov (Clinical trial number: NCT03350126). Written informed consent was obtained from all patients. All patients included in C1 received anti-PD1 (nivolumab) + anti-CTL4 (ipilumumab). Concerning

ImmunoMSI prospective cohort (C2) [25], all consecutive MSI/dMMR mCRC patients treated with ICI (anti-PD-1 monotherapy or anti-PD-1 plus anti-CTLA-4 combination) at Saint-Antoine Hospital, Medical Oncology department (Prof. Thierry André) from February 2015 to December 2019, were included. This research was approved by the ethics committee (N°2020 – CER 2020-6). The identification numbers of the ethic committees are the following, i.e., CPP N°2017/45 (ANSM reference: 170508A-12; EudraCT N°2017-002442-72) for C1 NIPICOL clinical trial and CPP N°2020 CER 2020-6C2 for ImmunoMSI. The Nipicol trial NCT03350126 has been completed and its primary endpoint published [14].

Assessment of microsatellite status

All CRC samples from C1, C2 and other cohorts used in this post-hoc study were centrally reassessed for MSI and dMMR status using immunohistochemistry (IHC) and for MSI using polymerase chain reaction (PCR) as described [26, 27]. Next, MSIsensor (version 0.6) and MSICare were used by default on paired normal-tumor exome data, to evaluate the mutation status of microsatellites using considering the whole exome data. MSIsensor score threshold of 10% or more was used to classify the MSI-H tumor (MSI-High) and a MSICare threshold of 20% was used to define MSI status as previously described [28].

Radiological analyses

Tumors were assessed ≤ 28 days before the first dose (baseline) and every 6 to 10 weeks, thereafter, according to different protocols. The decision to pursue treatment beyond iuPD was at the discretion of the treating physician. Treatment beyond iuPD was conditional to a confirmatory imaging 4 to 8 weeks after the first evidence of progression. Imaging was retrospectively and centrally reviewed by an experienced radiologist according to RECIST1.1 and iRECIST. [29]. Radiological progression was defined as confirmed PD (cPD) according to iRECIST 1.1. All cases of PD and pseudo progression were reviewed by a second experienced radiologist unaware of the target and non-target lesions chosen by the first radiologist. In case of discrepancy, a final decision was reached by consensus.

Survival analysis of ICI treated patients

Survival analysis on ICI patients was performed from the date of first infusion of any ICI. iPFS by iRECIST [29] was calculated from the first dose to the first documented cPD, or death resulting from any cause, whichever occurred first. Kaplan Meier curves were used to visualize difference in progression free survival (iPFS) between patients' groups diverging on genomic instability (e.g., TMB-High or MSISensor-High or MSICare-High,>20th percentile; TMB-Low or MSISensor-Low or MSICare-low ≤20th percentile) or to show at the selected cutoff values a clinical effect of our DNA or RNA signatures. The cutoff values were selected to optimize the clinical effect of our DNA or RNA signatures on ICI response in patients. Nevertheless, the validity of same signatures was also tested without using cutoff values with Cox models, similarly showing a clinical relevance, as indicated in the corresponding figures. The use of the cutoffs has been envisioned more to illustrate the findings but there is no dependence on these cutoffs for the demonstration of the clinical impact of both the DNA and RNA signatures. Two-sided Log-rank test was performed using the R package Survival (version 3.2.3).

P-value levels and Correction of *p*-values

In all statistical analyses, *p*-value ≤ 0.05 (risk alpha) was used as a threshold of significance. As an exception, for the selection of DNA variants following WES in C1, *p*-value ≤ 0.1 has been applied in order to provide pre-selection of a larger number of DNA variants prior to validation of their putative clinical significance in C2 by targeted sequencing (reduction of the risk of false negatives).

We systematically applied multi-test correction using Benjamini-Hochberg's method to control the false discovery rate when multiple tests of the same hypotheses were performed. However, we chose to highlight either one or the other either for clarity or fairness of comparison. We systematically presented uncorrected and corrected *p*-values when relevant in each of the corresponding figures and supplementary figures.

Data availability

The processed datasets used in the current study are now available in the github repository, https://github.com/CRSA-MSI/R-ICI_MNB_Survival. Reasonable request for sharing biologic materials or raw data files will be reviewed by the corresponding author (ADu). Patient- related data not included in the paper were generated as part of clinical trials and may be subject to patient confidentiality. Any data and materials that can be shared will be released via a material transfer agreement.

Code availability

The scripts and the Naive Bayes model can be accessed at GitHub https://github.com/CRSA-MSI/R-ICI_MNB_Survival. Scripts for ICA of RNA can be assessed at GitHub https://github.com/GeNeHetX/NipicolICA.

Concerning Sample preparation and sequencing, Exome Analysis and Mutational load, MHC class-I neoepitopes prediction, Feature selection and data pre-processing, DNA signatures (mutation count and Multinomial Naives Bayes), and Transcriptome profile generation and analysis, see **SUPPLEMENTARY MATERIALS AND METHODS.**

RESULTS

Patient population and study design

A total of 129 prospectively collected mCRC patients were assessed for eligibility, including 57 patients from the NIPICOL clinical trial (C1, NCT03350126) and 72 patients from the prospective ImmunoMSI cohort (C2) [25]. Clinical and disease characteristics of patients from C1 and C2 are summarized in **TABLE 1**, and further detailed in **SUPPLEMENTARY TABLE S1** and **SUPPLEMENTARY TABLE S2**. In C1, the analysis was restricted to 54 patients after removing 3 mCRC samples with misdiagnosed dMMR/MSI status (false positive cases that were in fact MSS). Whole Exome Sequencing (WES) and RNA Sequencing (RNASeq) were performed on 23 and 44 collected mCRC +/- matched normal colonic mucosa paraffin-embedded

samples, respectively, after removing 29 samples with lack of materials and/or insufficient quality (**FIG.1A**). In C2, targeted next-generation-sequencing (NGS) and RNASeq were performed on 66 and 72 mCRC +/- matched normal colonic mucosa paraffin-embedded samples, respectively, after removing unqualified samples for similar reasons, i.e., insufficient quantity and/or low-quality level (**FIG.1A**). The CONSORT-like clinical and molecular diagram in **FIGURE 1** outlines the methodology workflow of the study.

FIGURE 1 also summarizes the flow chart (**FIG. 1A**) and the current design of the study (**FIG. 1B**). In brief, NIPICOL (C1) was used as a training and ImmunoMSI (C2) as a validation cohort. Progression-free survival (PFS) by iRECIST (RECIST for Response Evaluation Criteria in Solid Tumor) (iPFS) [29] was used as primary endpoint. In an effort to optimize the available clinical data for the purpose of identifying available RNA/DNA predictive markers of resistance to ICI in this prospective series of ICI-treated patients with MSI mCRC, their putative clinical relevance was examined in C1 (training set) and yet in C2 (validation set) independently. C1 was a cohort from a clinical trial including dMMR/MSI patients all treated with the same treatment, i.e., a combination of nivolumab (anti-PD-1) and ipilimumab (anti-CTLA-4) after failure of standards of care. C2 was a larger and more heterogeneous cohort concerning regimen of ICI received (anti-PD1 alone or associated with ipilimumab) and inclusion criteria were less restrictive compared to a clinical trial.

The level of MSI and TMB in tumor DNA does not predict response to ICI in patients following exclusion of ICI-treated mCRC with misdiagnosed dMMR/MSI status

We first focused DNA analyses on the genomic quantitative indexes that are related to MSI in tumor DNA, i.e., the TMB and MSIsensor score, whose level was previously reported to predict response to ICI in patients with metastatic dMMR tumor [15, 16] (**SUPPLEMENTARY FIGURE S1**). Our data establish in this study that there is no influence of MSISensor score nor TMB on the iPFS of patients from C1 after exclusion of the cases with false positive MSI status (that were MSS, n = 3 and may lead to wrongly give a prognostic value to TMB and/or MSISensor regarding iPFS, see **SUPPLEMENTARY FIGURE S1**) (**FIG. 2C**). As shown also in **SUPPLEMENTARY FIGURE S1**, the MSICare score is no more clinically relevant for predicting iPFS to ICI

in patients with confirmed MSI mCRC, nor is the number of neoepitopes presented by autologous class I HLA alleles when calculated using a dedicated pipeline which combines several software [30-33]. In view of these results, we decided not to investigate further the clinical relevance of MSIsensor score, TMB and number of neoepitopes in C2 since none of them were associated with patients' prognosis in a true MSI mCRC population.

Identification of a 19-plex MSI signature predictive of response to ICI in mCRC patients

We first examined by WES the impact of somatic variants occurring in true positive MSI mCRC patients from C1 regarding iPFS upon ICI treatment. Expectedly, a great number of variants occurred at both nonrepetitive (NR, in n = 3,886 genes, only coding events) or repetitive (R, in n = 20,472 microsatellite-containing genes, both coding or noncoding events) sequences in genes having or not an expected role in the MSI-driven tumorigenic process. For survival analyses, we considered only somatic microsatellite mutations in tumor DNAs, because frequent hotspot NR mutations are rare in these tumors (**Fig. 2A** and **2B**). However, note that canonic NR mutations recurrently associated with colon tumor among which some were previously proposed to affect response to ICI, e.g., in *KRAS, BRAF, B2M* and other cancer-related genes, were not associated to iPFS in C1 (**SUPPLEMENTARY FIGURE S2**). In **FIGURE 2B** are shown the results of univariate cox analyses we performed to identify amongst the microsatellite variants the 167 alterations with impact on the iPFS of MSI mCRC patients in C1 ($p \leq 0.1$).

Like the NGS-based MSICare [28] or the PCR Pentaplex [26] genomic tools we previously designed, which use multiple microsatellite analysis to predict the MSI or MSS status of CRC, we hypothesized that response to ICI could be also predicted by investigating a set of selected microsatellite markers mutated in these tumors. From C1 (Training cohort), 19 candidate microsatellite markers (i.e., in *SUCO, LYST, MACO1, PPRC1, COMMD3, OCA2 MTMR10, IGDCC4, NLK, RNF43, TSEN54, ADGRE1, EDAR, TTN-AS1, IQCA1, RWDD4, CCDC158, CANX, MLIP*) were selected since: (i) their somatic mutations were each associated with iPFS in C1 (alpha = 5%) (**Fig 2A**) and (ii) their sequencing in C1 but also in additional public (TCGA COAD) and private cohorts (personal date, not shown) using NGS was successful in at least 95%

percent of tumors (**Fig 2A**) or in other words that these loci were particularly easy to analyze. A predictive nature of this 19-plex identified DNA signature based on the concomitant analysis of their microsatellite somatic variations in tumor DNA as compared to matched normal DNA was then evaluated by simply calculating for each patient the mean count of all the mutations in those microsatellites (**SUPPLEMENTARY FIGURE S3**). We also used Multinomial Naive Bayes (MNB) as a simple Machine Learning method to predict the risk of progression with the 19-plex signature [34]. We trained the MNB method on Nipicol (C1) and validated it on ImmunoMSI (C2). Applying the trained model in C2 (Validation cohort), we were able to show that the same 19-plex MSI signature was significantly associated to iPFS (HR_{C2} = 13.1; 95% CI [2.71-63.8] ; p = 1.4x10^{-3}) (**Fig 2B**). **FIGURE 2** further illustrates how the 19 microsatellite mutations contribute to predicting resistance to ICI in MSI mCRC patients (see the heatmap on **FIG. 2E**). In the multivariate analysis we conducted in C2 including molecular and clinical data (e.g., *KRAS* and *BRAF* mutation status) as well as the type of immunotherapy, the independent prognostic value of this 19-plex MSI signature was confirmed (HR_{C2} = 13.5; 95% CI [2.38-76.6] ; p = 3.3x10^{-3}) (**Fig. 2F**).

Transcriptomic signatures and response to ICI in MSI mCRC patients

Previous studies have provided evidence of the predictive value of RNA signature for immunotherapies. Three types of established signatures of response to ICI were systematically assessed in both discovery (C1) and validation (C2) cohorts: signatures quantifying cellular components of the tumor microenvironment (n=99), single gene expression levels (n= 19,116), and signaling pathway activity estimation from gene expression levels (n= 3,365). None of these established transcriptomic-based signature could be reproducibly associated to iPFS in the two ICI-treated MSI mCRC cohorts, including those specifically associated to ICI response in previous studies in MSS tumors (e.g., PD-1, PD-L1 +/- CTLA-4, T or B cells) (**SUPPLEMENTARY FIGURE S4**). More specifically, gene sets involved in angiogenesis, epithelial-to-mesenchymal transition, canonical TGF-beta and Wnt/Wingless signaling pathways, as well as TNF, interferon, KRAS or mTOR had either a minor and unreproduced association with iPFS

in only one cohort but more generally no significant correlation with survival in any of the two ICI-treated MSI mCRC cohorts (**SUPPLEMENTARY FIGURE S5**).

In order to identify context-dependent transcriptomic signatures (*i.e.,* phenotypic descriptors effectively observable in MSI mCRC), an unsupervised blind source separation approach was applied to the transcriptome profiles of the discovery cohort (C1; *i.e.*, independent component analysis; ICA) (**SUPPLEMENTARY FIGURE S6**). Only one of these components was associated to shorter iPFS in both C1 and C2 (HR_{C1} = 1.87 ; 95% CI [1.06-3.3] ; p = 0.0282 - HR_{C2} = 1.75 ; 95% CI [1.03-2.98] ; p = 0.035) (**Fig. 3B** and **3C** and **SUPPLEMENTARY FIGURE S6**). The component was significantly correlated to an RNA-based quantification of fibroblasts ($p < 0.001$) and anti-correlated to the tumor cellularity ($p < 0.001$) confirming its stromal origin (**FIG. 3A**, **SUPPLEMENTARY TABLE S3** for the list of genes most contributing to this stromal component). This fibrosis signature was associated to a tendon-like phenotype, extracellular matrix (ECM)-producing and interacting genes, enriched intra-tumor CMS4 proportions, and a pan-fibroblast TGF-β response signature (PMID: 29443960) (**FIG. 3A** and **SUPPLEMENTARY FIGURE S7**). The fibrosis signature was not related to stromal abundance, as measured by Sirius Red staining (**SUPPLEMENTARY FIGURE S8**). Exactly as this was previously performed with the DNA signature, we confirmed the independent prognostic value of this RNA signature using a multivariate analysis in C2 (HR_{C2} = 1.78 ; 95% CI [1.03-3.01] ; p = 0.040) (**Fig. 3D** and **SUPPLEMENTARY TABLE S1**). We successfully reduced this RNA signature to a more serviceable set of 182 biomarkers (**SUPPLEMENTARY TABLE S4**). Using this raw sub panel, the spearman correlation with the original component was 0.98 in NIPICOL and 0.96 in immunoMSI (**SUPPLEMENTARY FIGURE S9)**. Both remained associated with iPFS as continuous scores. **SUPPLEMENTARY FIGURE S9** shows the Kaplan-Meier curves of iPFS using the same cut-off as with the original signature.

Multivariate Analyses combining the DNA and RNA signatures

We finally examined the effect of both RNA and DNA signatures in predicting iPFS to ICI in MSI mCRC patients using a multivariate model (**FIG. 4**). Either when taking into account both signatures in a continuous or a discrete way, the multivariate analysis indicated that both signatures were independently predictive of iPFS (**FIG. 4A**). **Figures**

4B (and SUPPLEMENTARY FIGURE S9) show how these DNA and RNA signatures are complementary and effective when used together in predicting the response of patients to ICI treatment. One and/or another of the signatures was able to predict progression in patients from C2 regarding iPFS to ICI (HR_{C2} = 6.0 ; 95% CI [1.80 – 19.9] $p = 9.12x10^{-4}$). This makes these signatures a valuable classifier tool capable of predicting relapse in MSI mCRC patients (see also on SUPPLEMENTARY FIGURE S10 the performance of this combined analysis when the RNA stromal signature was reduced to 182 markers).

DISCUSSION

In this study, we examine the issue of response to ICI in patients with dMMR/MSI mCRC. Two prospective cohorts of patients are examined to investigate this question. The study is limited to CRC patients only, thus avoiding the risk that the origin of the primary tumor might interfere with the results. The dual approach of high-throughput analysis of tumor DNA and RNA enables us to perform both supervised and unsupervised analyses in the aim of investigating ICI-response associated genotypes and phenotypes. Note worthily, the dMMR/MSI status of the tumors was systematically rechecked in our expert center as part of this ancillary study to avoid misdiagnoses which can deeply impact the findings of such translational research studies, as reported [24, 35]. All these points constitute methodological strengths of the present work compared to others in the field which remain few and based on smaller number of patients.

We first show that several previously suggested DNA and RNA indicators are unlikely to have any robust predictive values regarding response to ICI in MSI mCRC patients. This is primarily the case for the quantitative DNA markers MSIsensor score and TMB [15, 16] when the diagnostic errors regarding the MSI status of the tumors are corrected upstream and false positive MSI cases with expected low MSIsensor score and TMB are therefore excluded. In addition, our analyses based on previously defined candidate DNA/RNA markers of resistance, e.g., specific somatic DNA variants, the activity of canonical signaling pathways or the presence of specific cellular contingents within the tumor bulk, also failed to identify robust predictors of ICI response in patients.

Though some of these markers may contribute to some extent to modulate the patients' response to ICI in some dMMR/MSI mCRC as suggested by some studies carried out on smaller series of patients, and more generally may be predictive of ICI efficacy in MMR proficient tumors, they are unlikely to have major clinical relevance.

The breakthrough results we have achieved in this study stem from the fact that we report and validate in both cohorts two distinct original signatures derived from a global analysis of the DNA and RNA profiles of ICI-treated MSI mCRC. In brief, the DNA signature is epithelial in nature. It analyzes the combination of a 19-plex panel aggregating independent somatic mutational events in dMMR tumor cells involving both coding and noncoding microsatellite containing-genes associated to distinct biological processes. As some microsatellite mutations such as those in the pentaplex are relevant for MSI diagnosis in CRC, the combined analysis of these 19 microsatellites is of predictive interest for response to ICI as evaluated by iPFS in patients. In addition, the RNA signature is stromal in nature. Though it is TGFB-related with a desmoplastic orientation, the fact that Sirius Red staining does not discriminate between samples with and without this stromal signature illustrates its complex nature. Note worthily, all the previously defined signatures and pathways that were shown to be associated to the proposed transcriptomic-defined TGFB-related fibrotic signature were not themselves associated to progression in both cohorts. This highlights the importance of defining context-dependent signatures, in particular in such distinct carcinogenic and microenvironment context as those found in MSI mCRC. In relation to a rich literature that has already provided evidence that the extracellular matrix and its heterogeneous content could promote resistance to ICI in MSS tumor models associated with various primary locations (for review see [36]), the RNA contingent we are identifying could thus play such a role by promoting, for example, immune-exclusion or sequestration processes in the context of increased fibrosis generated in and around the tumor. It could also modulate the response to treatment through non-mutually exclusive mechanisms involving more specifically the cancer-associated fibroblasts hosted in or responsible for the matrix generation.

Our work has some limitations. First, it does not address the issue of the choice of immunotherapy, i.e., monotherapy with anti-PD1 or combination of anti-PD1 and anti-CTL4, which is an important issue today. Second, the question of epigenetics is an

especially important issue that is not here addressed and will require further investigation in subsequent studies. Third, our work does not really shed light on simple mechanisms underlying resistance to ICI in MSI mCRC. In this respect, it is not yet very enlightening for the identification of novel therapeutic targets that could be of interest in the future for patients with primary or secondary resistance to anti-PD-1 ± anti-CTL4. Finally, although our results were established on a large prospective collection of patients including two independent cohorts, one of which is a clinical trial, they still require validation in new populations of metastatic MSI cancer patients, with colorectal tumor but possibly also other primary MSI cancer. Despite these weaknesses, the 2 signatures we outline here from the analysis of the tumor bulk are easy to investigate and can be implemented in the context of a clinical routine; the DNA signature requires the analysis of the status of only 19 microsatellite markers within the tumor, ideally by NGS but possibly also by other methods while the RNA signature requires to perform 3'RNA-sequencing which is a simple, reproducible and feasible method to be used with paraffin-embedded tumor samples, the cost of which has now decreased considerably. Of interest, we demonstrate that the RNA signature reduced to 182 markers is still clinically relevant for predicting iPFS to ICI. Finally, it is very interesting to note that the DNA and RNA signatures have independent predictive value and can be used jointly to predict progression in ICI-treated MSI mCRC patients. This should be of interest for the design of future strategies improving ICI for MSI cancer patients in clinics.

REFERENCES

1 Ionov Y, Peinado MA, Malkhosyan S et al. Ubiquitous somatic mutations in simple repeated sequences reveal a new mechanism for colonic carcinogenesis. Nature 1993; 363 (6429): 558-561.

2 Aaltonen LA, Peltomaki P, Leach FS et al. Clues to the pathogenesis of familial colorectal cancer. Science 1993; 260 (5109): 812-816.

3 Fishel R, Lescoe MK, Rao MR et al. The human mutator gene homolog MSH2 and its association with hereditary nonpolyposis colon cancer. Cell 1993; 75 (5): 1027-1038.

4 Svrcek M, Lascols O, Cohen R et al. MSI/MMR-deficient tumor diagnosis: Which standard for screening and for diagnosis? Diagnostic modalities for the colon and other sites: Differences between tumors. Bull Cancer 2019; 106 (2): 119-128.

5 Hamelin R, Chalastanis A, Colas C et al. [Clinical and molecular consequences of microsatellite instability in human cancers]. Bull Cancer 2008; 95 (1): 121-132.

6 Duval A, Hamelin R. Mutations at coding repeat sequences in mismatch repair-deficient human cancers: toward a new concept of target genes for instability. Cancer Res 2002; 62 (9): 2447-2454.

7 Llosa NJ, Cruise M, Tam A et al. The vigorous immune microenvironment of microsatellite instable colon cancer is balanced by multiple counter-inhibitory checkpoints. Cancer Discov 2015; 5 (1): 43-51.

8 Le DT, Uram JN, Wang H et al. PD-1 Blockade in Tumors with Mismatch-Repair Deficiency. N Engl J Med 2015; 372 (26): 2509-2520.

9 Cohen R, Colle R, Pudlarz T et al. Immune Checkpoint Inhibition in Metastatic Colorectal Cancer Harboring Microsatellite Instability or Mismatch Repair Deficiency. Cancers (Basel) 2021; 13 (5).

10 Andre T, Shiu KK, Kim TW et al. Pembrolizumab in Microsatellite-Instability-High Advanced Colorectal Cancer. N Engl J Med 2020; 383 (23): 2207-2218.

11 Le DT, Durham JN, Smith KN et al. Mismatch repair deficiency predicts response of solid tumors to PD-1 blockade. Science 2017; 357 (6349): 409-413.

12 Overman MJ, McDermott R, Leach JL et al. Nivolumab in patients with metastatic DNA mismatch repair-deficient or microsatellite instability-high colorectal cancer (CheckMate 142): an open-label, multicentre, phase 2 study. Lancet Oncol 2017; 18 (9): 1182-1191.

13 Overman MJ, Lonardi S, Wong KYM et al. Durable Clinical Benefit With Nivolumab Plus Ipilimumab in DNA Mismatch Repair-Deficient/Microsatellite Instability-High Metastatic Colorectal Cancer. J Clin Oncol 2018; 36 (8): 773-779.

14 Cohen R, Bennouna J, Meurisse A et al. RECIST and iRECIST criteria for the evaluation of nivolumab plus ipilimumab in patients with microsatellite

instability-high/mismatch repair-deficient metastatic colorectal cancer: the GERCOR NIPICOL phase II study. J Immunother Cancer 2020; 8 (2).

15 Mandal R, Samstein RM, Lee KW et al. Genetic diversity of tumors with mismatch repair deficiency influences anti-PD-1 immunotherapy response. Science 2019; 364 (6439): 485-491.

16 Schrock AB, Ouyang C, Sandhu J et al. Tumor mutational burden is predictive of response to immune checkpoint inhibitors in MSI-high metastatic colorectal cancer. Ann Oncol 2019; 30 (7): 1096-1103.

17 Gurjao C, Liu D, Hofree M et al. Intrinsic Resistance to Immune Checkpoint Blockade in a Mismatch Repair-Deficient Colorectal Cancer. Cancer Immunol Res 2019; 7 (8): 1230-1236.

18 Chida K, Kawazoe A, Suzuki T et al. Transcriptomic Profiling of MSI-H/dMMR Gastrointestinal Tumors to Identify Determinants of Responsiveness to Anti-PD-1 Therapy. Clin Cancer Res 2022; 28 (10): 2110-2117.

19 Kwon M, An M, Klempner SJ et al. Determinants of Response and Intrinsic Resistance to PD-1 Blockade in Microsatellite Instability-High Gastric Cancer. Cancer Discov 2021; 11 (9): 2168-2185.

20 Bortolomeazzi M, Keddar MR, Montorsi L et al. Immunogenomics of Colorectal Cancer Response to Checkpoint Blockade: Analysis of the KEYNOTE 177 Trial and Validation Cohorts. Gastroenterology 2021; 161 (4): 1179-1193.

21 Chida K, Kawazoe A, Kawazu M et al. A Low Tumor Mutational Burden and PTEN Mutations Are Predictors of a Negative Response to PD-1 Blockade in MSI-H/dMMR Gastrointestinal Tumors. Clin Cancer Res 2021; 27 (13): 3714-3724.

22 Latham A, Srinivasan P, Kemel Y et al. Microsatellite Instability Is Associated With the Presence of Lynch Syndrome Pan-Cancer. J Clin Oncol 2019; 37 (4): 286-295.

23 Germano G, Lu S, Rospo G et al. CD4 T Cell-Dependent Rejection of Beta-2 Microglobulin Null Mismatch Repair-Deficient Tumors. Cancer Discov 2021; 11 (7): 1844-1859.

24 Cohen R, Hain E, Buhard O et al. Association of Primary Resistance to Immune Checkpoint Inhibitors in Metastatic Colorectal Cancer With Misdiagnosis of

Microsatellite Instability or Mismatch Repair Deficiency Status. JAMA Oncol 2019; 5 (4): 551-555.

25 Colle R, Radzik A, Cohen R et al. Pseudoprogression in patients treated with immune checkpoint inhibitors for microsatellite instability-high/mismatch repair-deficient metastatic colorectal cancer. Eur J Cancer 2021; 144: 9-16.

26 Buhard O, Cattaneo F, Wong YF et al. Multipopulation analysis of polymorphisms in five mononucleotide repeats used to determine the microsatellite instability status of human tumors. J Clin Oncol 2006; 24 (2): 241-251.

27 Buhard O, Lagrange A, Guilloux A et al. HSP110 T17 simplifies and improves the microsatellite instability testing in patients with colorectal cancer. J Med Genet 2016; 53 (6): 377-384.

28 Ratovomanana T, Cohen R, Svrcek M et al. Performance of Next-Generation Sequencing for the Detection of Microsatellite Instability in Colorectal Cancer With Deficient DNA Mismatch Repair. Gastroenterology 2021; 161 (3): 814-826 e817.

29 Seymour L, Bogaerts J, Perrone A et al. iRECIST: guidelines for response criteria for use in trials testing immunotherapeutics. Lancet Oncol 2017; 18 (3): e143-e152.

30 Boegel S, Lower M, Schafer M et al. HLA typing from RNA-Seq sequence reads. Genome Med 2012; 4 (12): 102.

31 Hundal J, Kiwala S, McMichael J et al. pVACtools: A Computational Toolkit to Identify and Visualize Cancer Neoantigens. Cancer Immunol Res 2020; 8 (3): 409-420.

32 Lundegaard C, Lamberth K, Harndahl M et al. NetMHC-3.0: accurate web accessible predictions of human, mouse and monkey MHC class I affinities for peptides of length 8-11. Nucleic Acids Res 2008; 36 (Web Server issue): W509-512.

33 Reynisson B, Alvarez B, Paul S et al. NetMHCpan-4.1 and NetMHCIIpan-4.0: improved predictions of MHC antigen presentation by concurrent motif deconvolution and integration of MS MHC eluted ligand data. Nucleic Acids Res 2020; 48 (W1): W449-W454.

34 Abraham A, Pedregosa F, Eickenberg M et al. Machine learning for neuroimaging with scikit-learn. Front Neuroinform 2014; 8: 14.

35 Loupakis F, Depetris I, Biason P et al. Prediction of Benefit from Checkpoint Inhibitors in Mismatch Repair Deficient Metastatic Colorectal Cancer: Role of Tumor Infiltrating Lymphocytes. Oncologist 2020; 25 (6): 481-487.

36 O'Donnell JS, Teng MWL, Smyth MJ. Cancer immunoediting and resistance to T cell-based immunotherapy. Nat Rev Clin Oncol 2019; 16 (3): 151-167.

37 Powles T, Kockx M, Rodriguez-Vida A et al. Clinical efficacy and biomarker analysis of neoadjuvant atezolizumab in operable urothelial carcinoma in the ABACUS trial. Nat Med 2019; 25 (11): 1706-1714.

FIGURE LEGENDS

Table 1: Patients description from C1 and C2 cohorts with main corresponding clinical data

Figure 1: Workflow and Study Design

MSS, microsatellite stable; mCRC, metastatic colorectal cancer; ICI, immune checkpoint inhibitors; IHC, Immunohistochemistry; QC, quality control; pMMR, mismatch repair proficient.

Figure 2: Identification of a 19-plex MSI signature predictive of response to ICI in mCRC patients

A) Histogram of *p*-values from cox analysis for R variants (microsatellites) in the C1 Nipicol cohort. A zoom was performed on those having a *p*-value lower than 0.1 (n = 167). Genes' name of the 19 somatic MS variants with a known percentage of missing data < 5% in C1 and other public and private cohorts are indicated in green. They were used further for investigating iPS to ICI in C2.
B) Counts of microsatellite somatic variants according to their *p*-value (uni-variate Cox regression model) on the 23 patients of Nipicol (C1). Green and red bar represent the mutated microsatellites with a *p*-value < 0.05 and 0.05 ≤ *p*-value < 0.1, respectively. The top forestplot represent in C2 the Cox survival regression results on model prediction of risk output, represented by the hazard ratio (HR < 1 : beneficial, HR = 1 No effect, HR > 1 : deleterious). High (*p*-value < 0.05, DNA signature) in green vs low stringency of Cox features selection based on *p*-value in red.
C) iPFS curve for the TMB and the MSIsensore score.
D) Kaplan-Meier curves of iPFS are shown accordingly to risk probability in ImmunoMSI only (n= 66). Red curve corresponds to patients with high MNB probability (<20%) and blue curve corresponds to patients with low MNB probability (>20%).
E) Heatmap representation of NIPICOL (C1) and ImmunoMSI (C2). Overview of mutations profile for each patient on the list of 19 selected microsatellites (MS, see

genes' name and chromosomal location on the left). Bottom bars represent their treatment (combo-therapy or mono-therapy), survival (time-to-event), event (Progressor or Non-Progressor), DNA.signature (probabilty of non-response according to iPFS given by the MNB), KRAS and BRAF mutational status. Patients are ordered based on predicted risk of progress and MS are ordered in function of mutation frequency in Nipicol cohort.

F) Forest plot of the multivariate Cox regression with iPFS in cohort C2, with its corresponding *p*-value. Included features are DNA signature (low to high risk), BRAF, KRAS (wild-type vs mutated status) and treatment (mono vs. combo).

Figure 3: Transcriptomic signatures and response to ICI in MSI mCRC patients

A) Heatmap of the stromal signature, patients (in column) are ordered by the estimated quantification of the stromal ICA signature. iRECIST status of patients [29] are shown along with gene-wise centered expression values of the gene most associated to the component, tumor purity estimated by the non-repeated variant allele frequency, MCPcounter -based fibroblast quantification estimate, the main CMS (consensus molecular subtype) and the intra-tumoral proportion estimate of CMS4, and TGFB response signature [37]. Pathway-level activity estimate are also shown along with the Gene Set Enrichment Analysis estimates.

B) Univariate association with progression-free survival in Nipicol (C1, n=44) or ImmunoMSI (C2, n=71) of the continuous score of the signature or of a classification using the third quartile as a threshold (Q3 cut-off).

C) Kaplan-Meier estimates using the third quantile threshold of the stromal signature.

D) Forest plot of the multivariate Cox regression with progression-free survival in cohort C2, representing hazard ratio (HR < 1 : beneficial, HR = 1 No effect, HR > 1 : deleterious) with its corresponding *p*.value. Included features are stromal signature (low to high), BRAF, KRAS (wild-type vs mutated), and treatment (mono vs. combo).

Figure 4: Multivariate Analyses combining the DNA and RNA signatures

A) Forestplot of the RNA or DNA signatures as well as the treatment type considering the continuous value (upper panel) or by discretizing the values (lower panel) of the signatures.

B) Kaplan-Meier estimates of iPFS as a function of the intensity combination of the two signatures (n=66). High RNA and DNA signatures are shown in red. Low RNA and DNA signatures are shown in green. High RNA signature and weak DNA signature are shown in orange and low RNA signature and high DNA signature are shown in purple.

A. Worflow

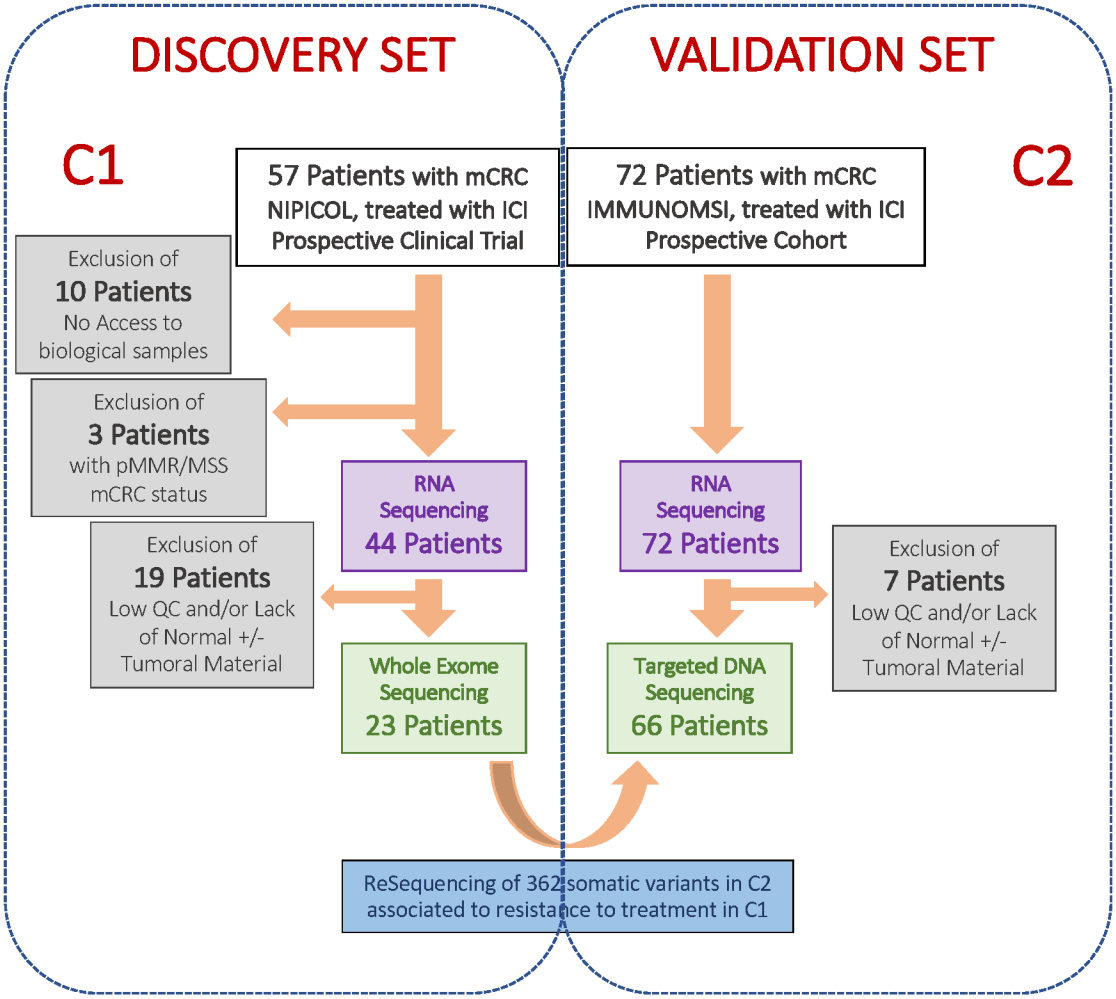

B. Study Design

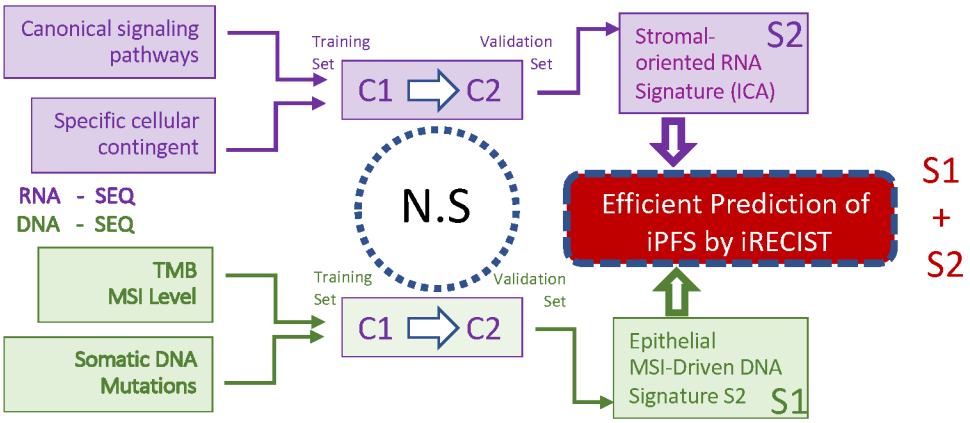

Figure 1

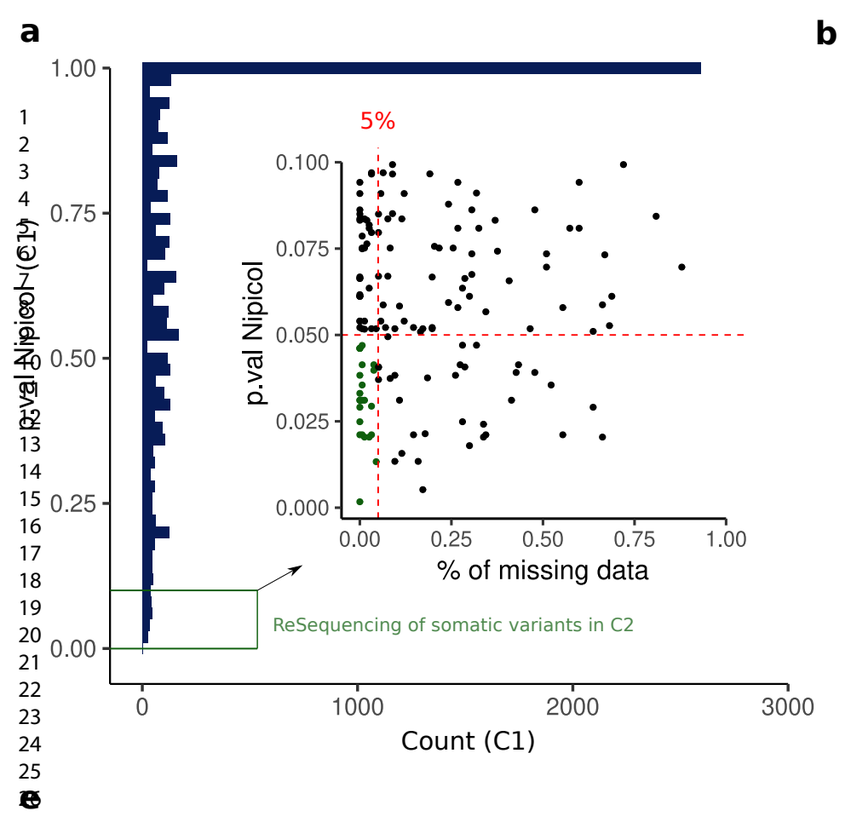

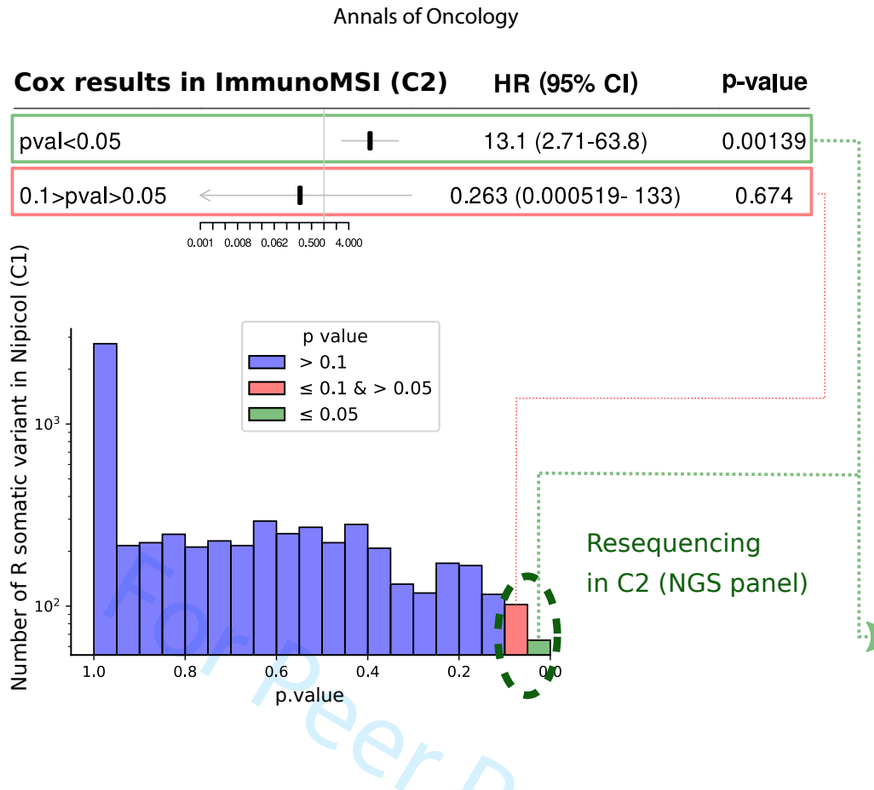

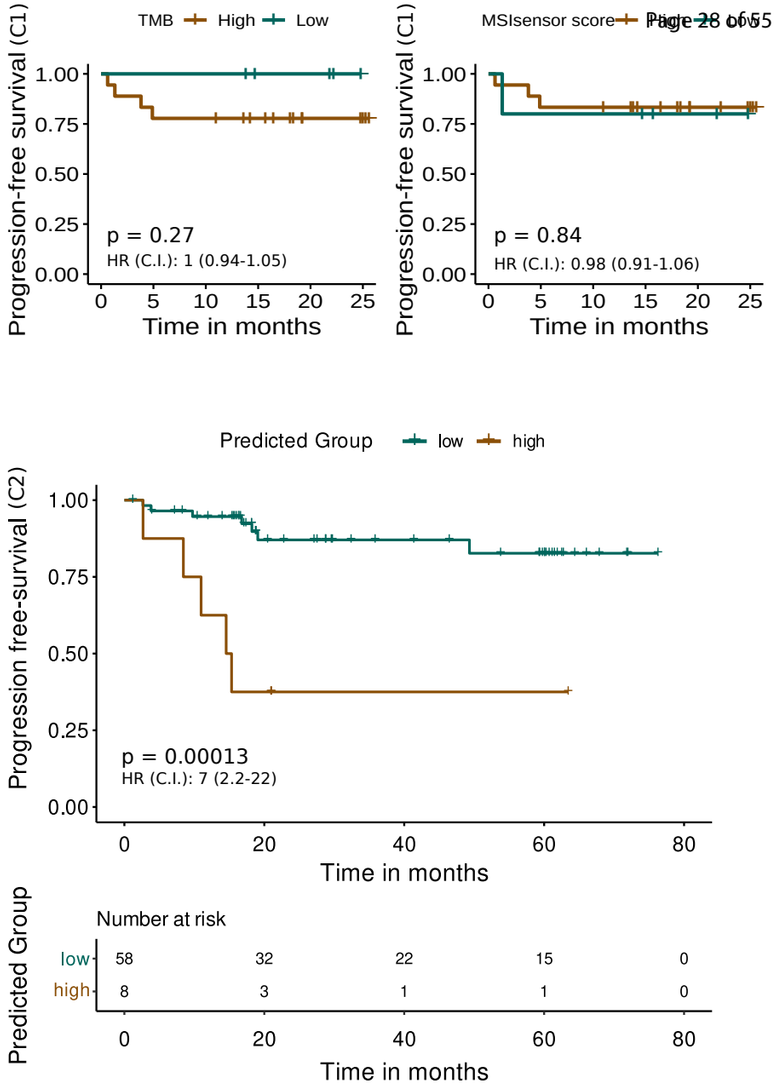

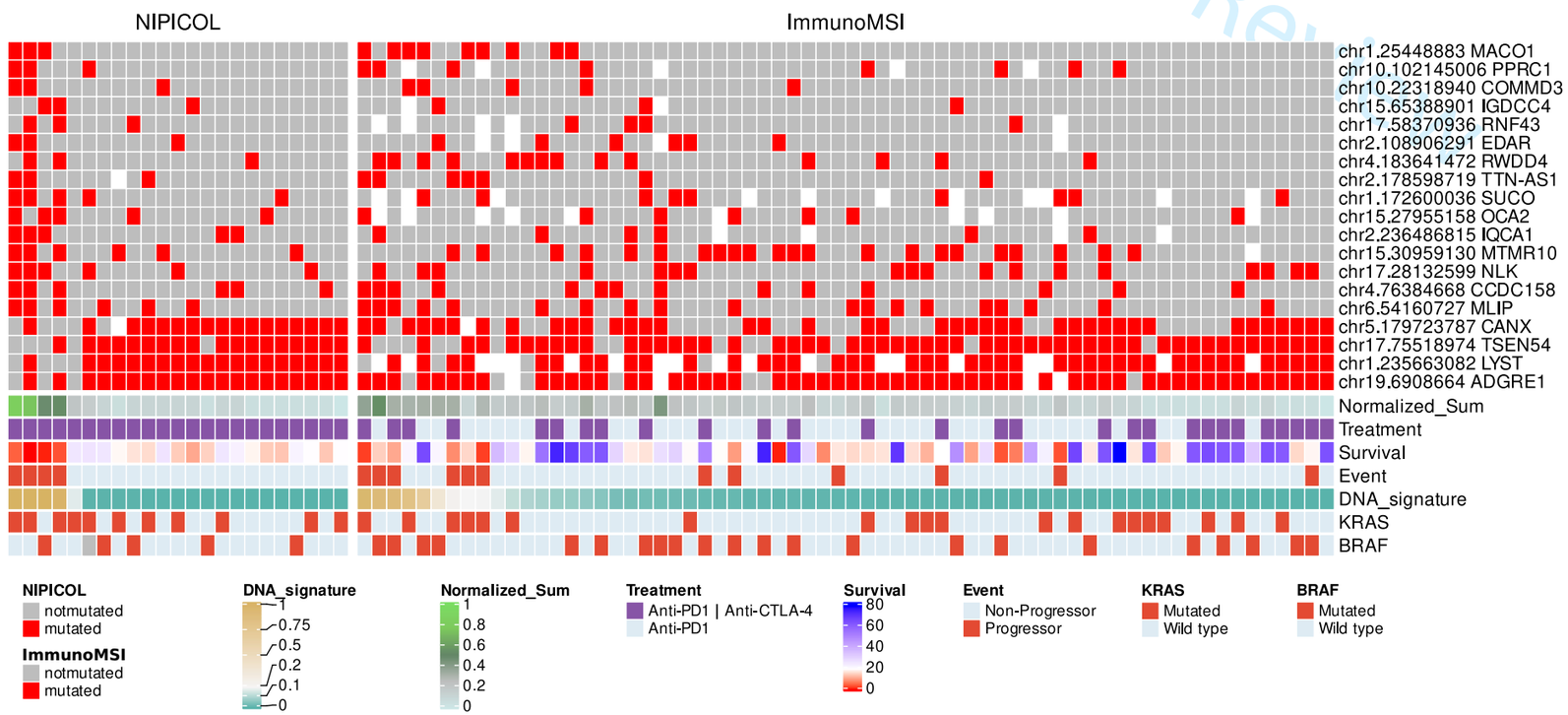

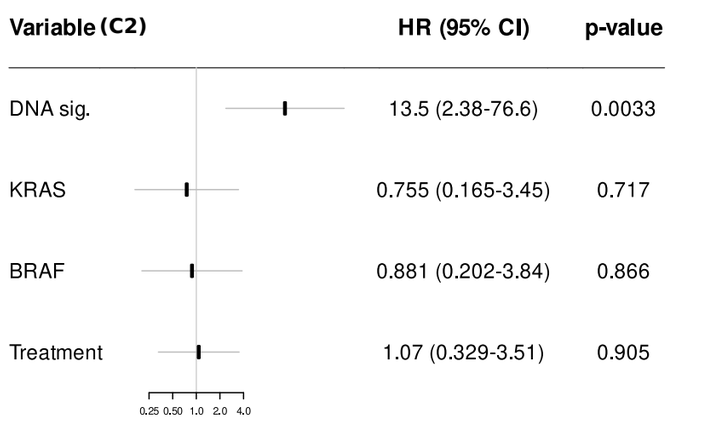

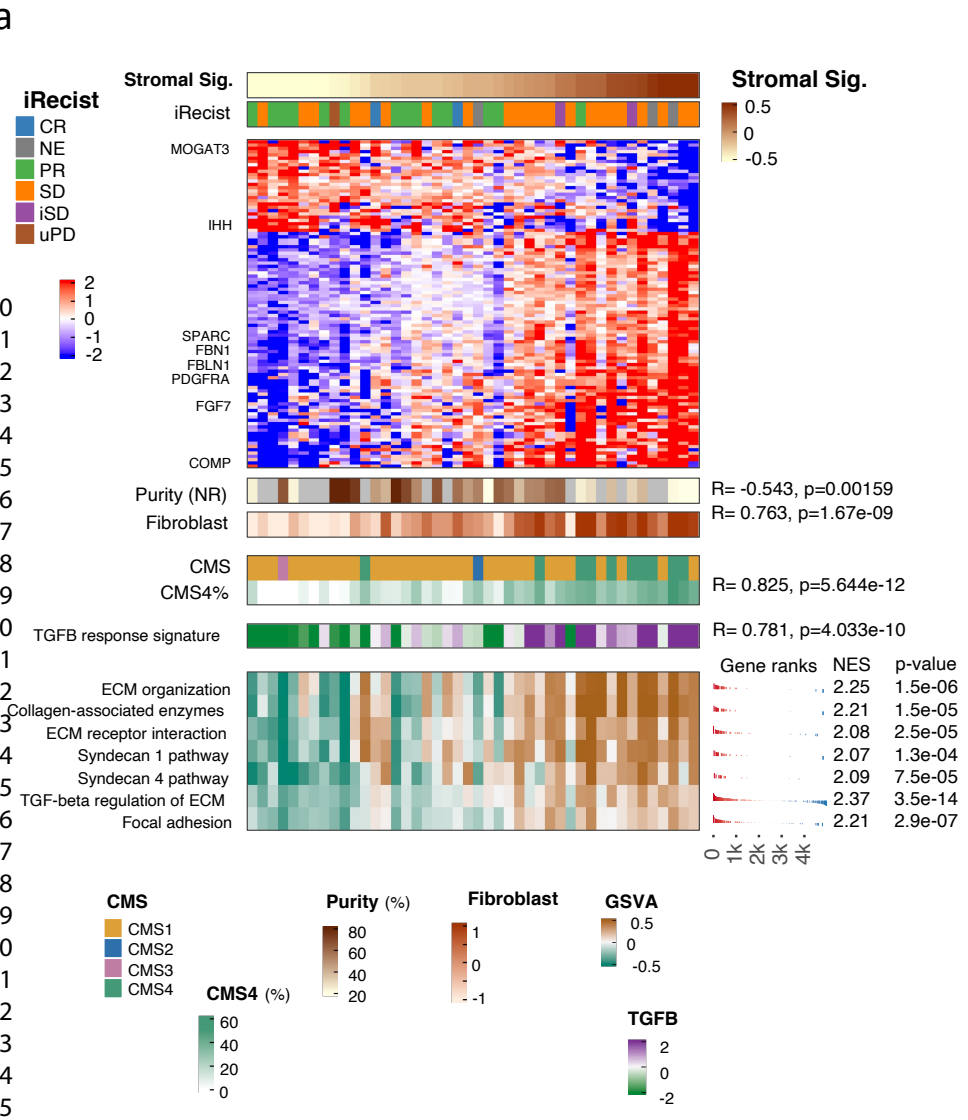

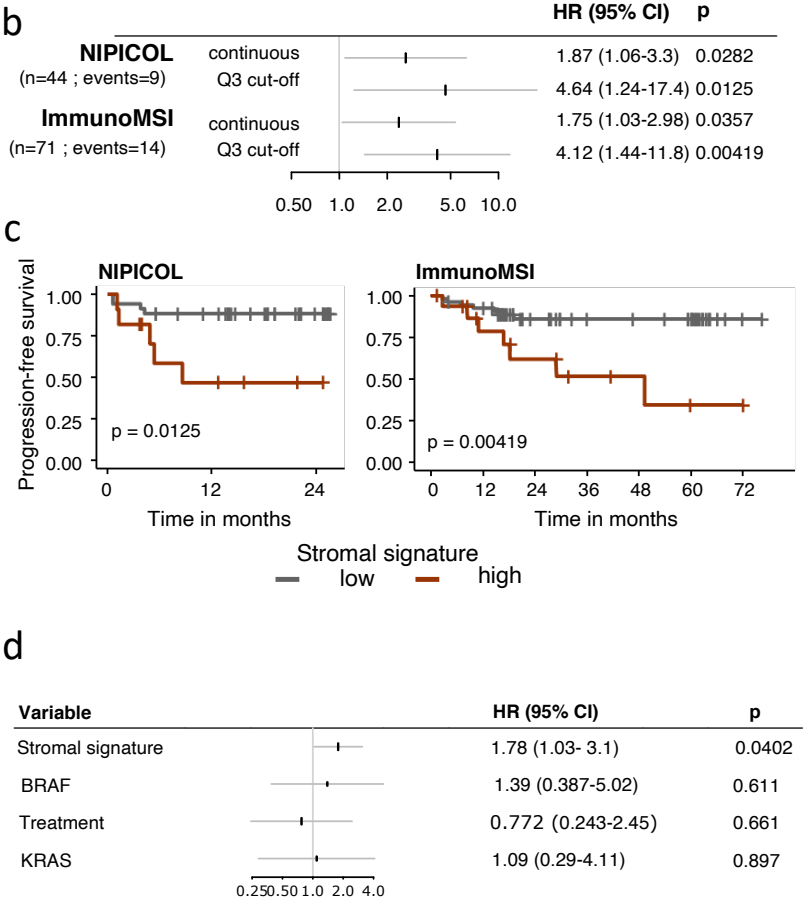

d

Variable	HR (95% CI)	p
Stromal signature	1.78 (1.03- 3.1)	0.0402
BRAF	1.39 (0.387-5.02)	0.611
Treatment	0.772 (0.243-2.45)	0.661
KRAS	1.09 (0.29-4.11)	0.897

Figure 3

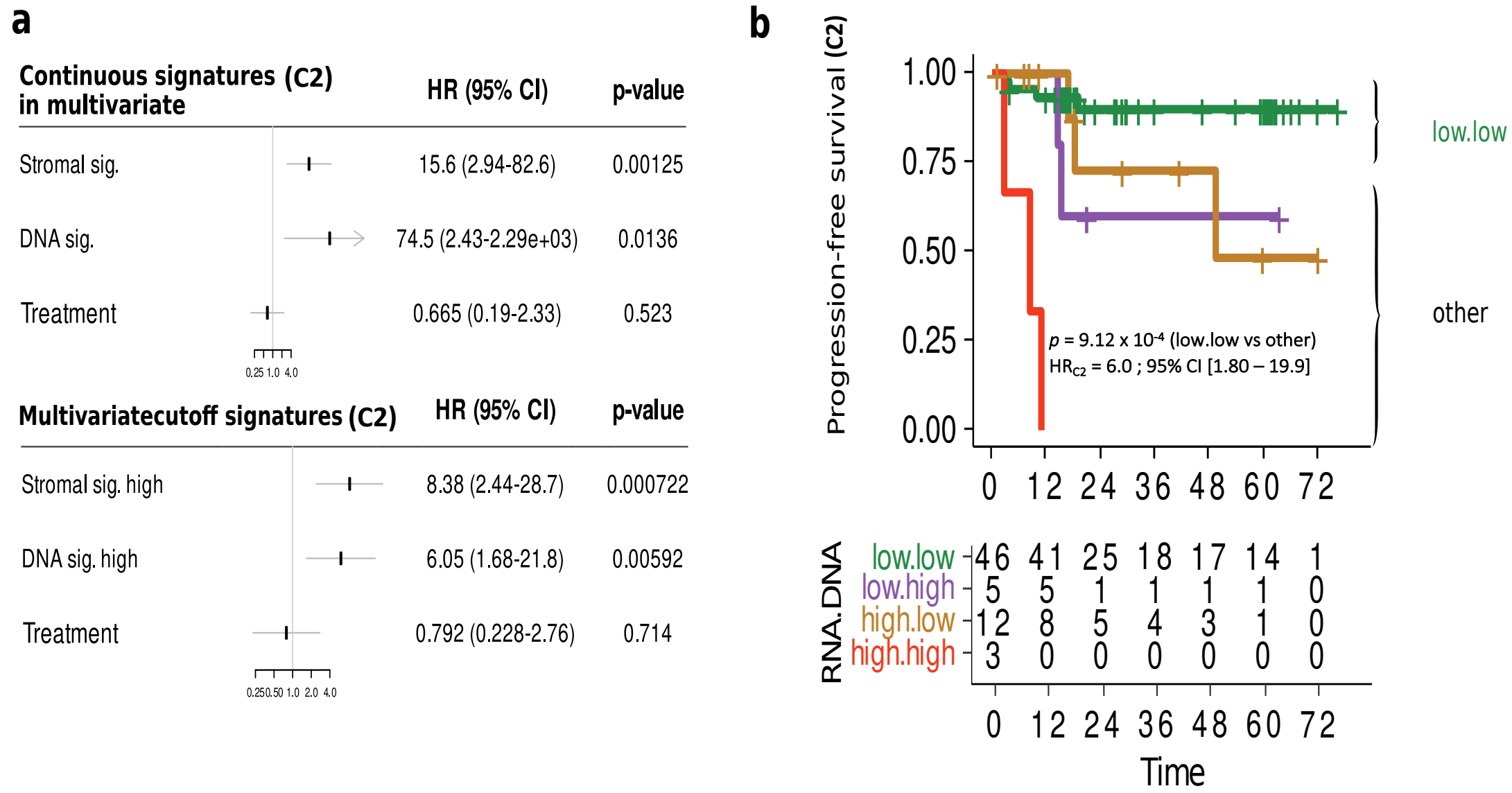
a
Continuous signatures (C2) in multivariate
HR (95% CI)
p-value
Stromal sig.
15.6 (2.94-82.6)
0.00125
DNA sig.
74.5 (2.43-2.29e+03)
0.0136
Treatment
0.665 (0.19-2.33)
0.523
0.25 1.0 4.0
Multivariatecutoff signatures (C2)
HR (95% CI)
p-value
Stromal sig. high
8.38 (2.44-28.7)
0.000722
DNA sig. high
6.05 (1.68-21.8)
0.00592
Treatment
0.792 (0.228-2.76)
0.714
0.25 0.50 1.0 2.0 4.0
b
Progression-free survival (C2)
1.00
0.75
0.50
0.25
0.00
p = 9.12 x 10-4 (low.low vs other)
HRC2 = 6.0 ; 95% CI [1.80 – 19.9]
low.low
other
0 12 24 36 48 60 72
RNA.DNA
low.low 46 41 25 18 17 14 1
low.high 5 5 1 1 1 1 0
high.low 12 8 5 4 3 1 0
high.high 3 0 0 0 0 0 0
0 12 24 36 48 60 72
Time

Figure 4

Characteristic	ImmunoMSI, N = 72[1]	Nipicol, N = 47[1]	p-value[2]
Age in Yrs	59 (15)	54 (13)	0.058
Sex			0.87
Female/Male	28/44	19/28	
ECOG performance score			0.24
0/≥1/Unknown	35/36/1	18/29/0	
Primary tumor location			0.49
Left colon/ Right colon/Unknown	23/47/2	18/28/1	
BRAFV600E			0.056
Mutated/ Wild type/Unknown	23/49/0	7/37/3	
KRAS			0.029
Mutated/ Wild type	21/51	23/24	
NRAS			>0.99
Mutated/Wild type/Unknown	1/71/0	1/42/4	
Origin of MMR deficiency			0.82
Known germline mutation	20	27	
Sporadic/Unknown	10/42	12/8	
Surgery of primary tumor			>0.99
Yes/no/Unknown	71/1/0	43/1/3	
Number of metastatic sites			0.50
1 /2/ ≥3	27/26/19	14/18/15	
Number of prior lines			0.006
0/1/2/≥3	9/21/32/10	0/8/22/17	
Type of immunotherapy			<0.001
Anti-PD1/anti-PD1&CTLA4	43/29	0 / 47	
iRECIST			<0.001
CR/PR/SD/PD/NE	20/35/7/8/2	2/15/24/3/3	
Status			0.059
MSI/MSS	72 / 72 (100%)	44 / 3	

[1] Mean (SD); n / N (%)

[2] Wilcoxon rank sum test; Pearson's Chi-squared test; Fisher's exact test

Yrs: years; ECOG = Eastern Oncology Cooperative Group; MMR: Mismatch Repair; immune RECIST: iRECIST CR: complete response; PR: partial response; SD: stable disease; PD: progressive disease; MSI: microsatellite instability; MSS: microsatellite stable, NE: not evaluable

a

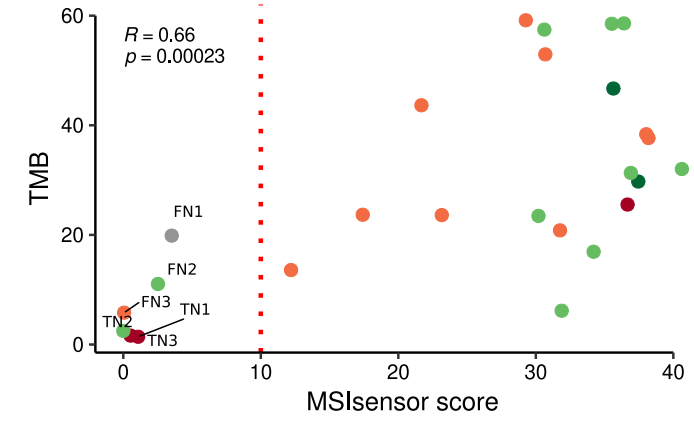

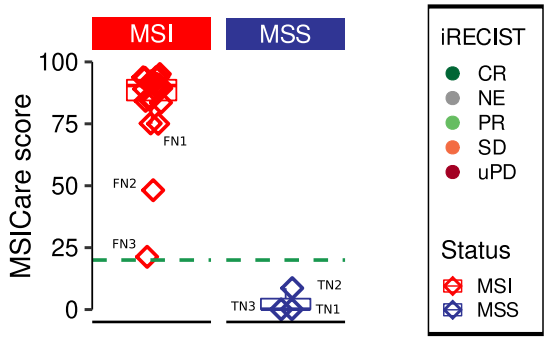

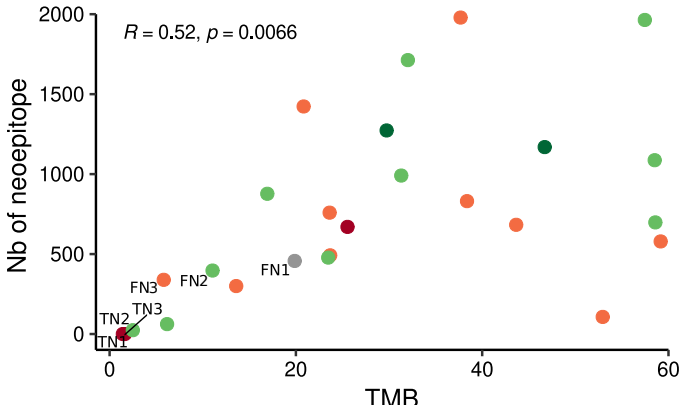

b

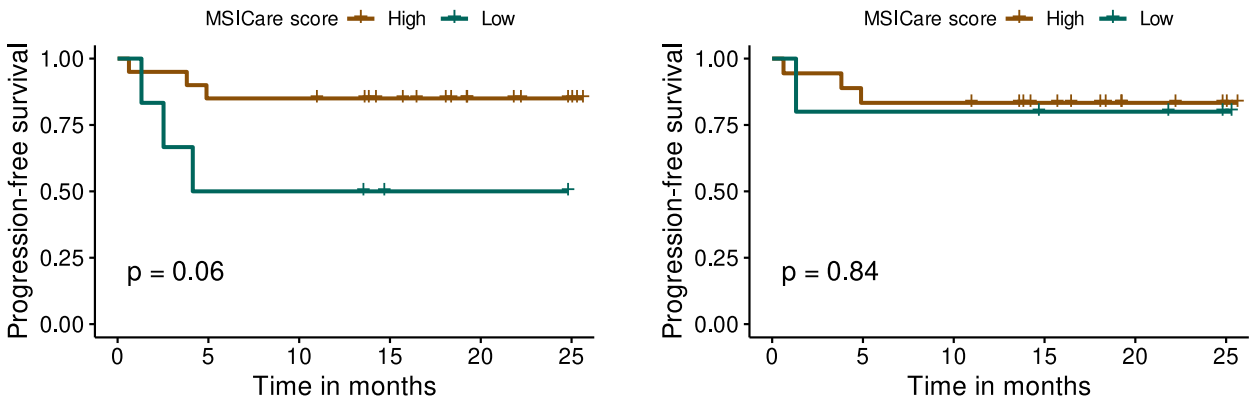

Before exclusion of MSS samples	HR (95% CI)	p-value
MSIsensor_score	0.963 (0.914-1.02)	0.165
TMB	0.975 (0.93-1.02)	0.282
Neoepitope	0.999 (0.997- 1)	0.3

After exclusion of MSS samples	HR (95% CI)	p-value
MSIsensor_score	0.984 (0.912-1.06)	0.672
Neoepitope	1 (0.998- 1)	0.807
TMB	0.995 (0.94-1.05)	0.876

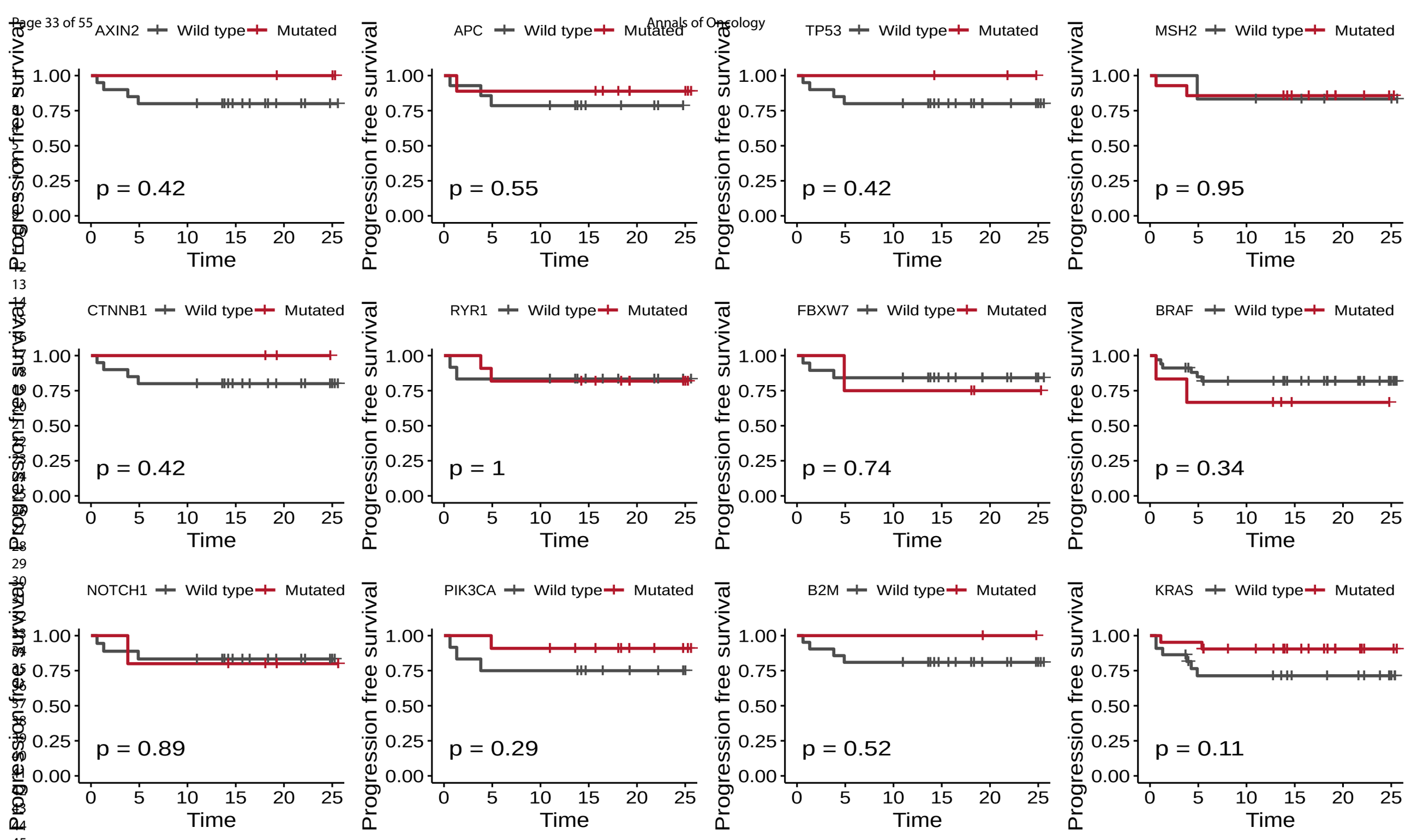
AXIN2 Wild type Mutated
p = 0.42
APC Wild type Mutated
p = 0.55
TP53 Wild type Mutated
p = 0.42
MSH2 Wild type Mutated
p = 0.95
CTNNB1 Wild type Mutated
p = 0.42
RYR1 Wild type Mutated
p = 1
FBXW7 Wild type Mutated
p = 0.74
BRAF Wild type Mutated
p = 0.34
NOTCH1 Wild type Mutated
p = 0.89
PIK3CA Wild type Mutated
p = 0.29
B2M Wild type Mutated
p = 0.52
KRAS Wild type Mutated
p = 0.11
Progression free survival
1.00
0.75
0.50
0.25
0.00
0
5
10
15
20
25
Time

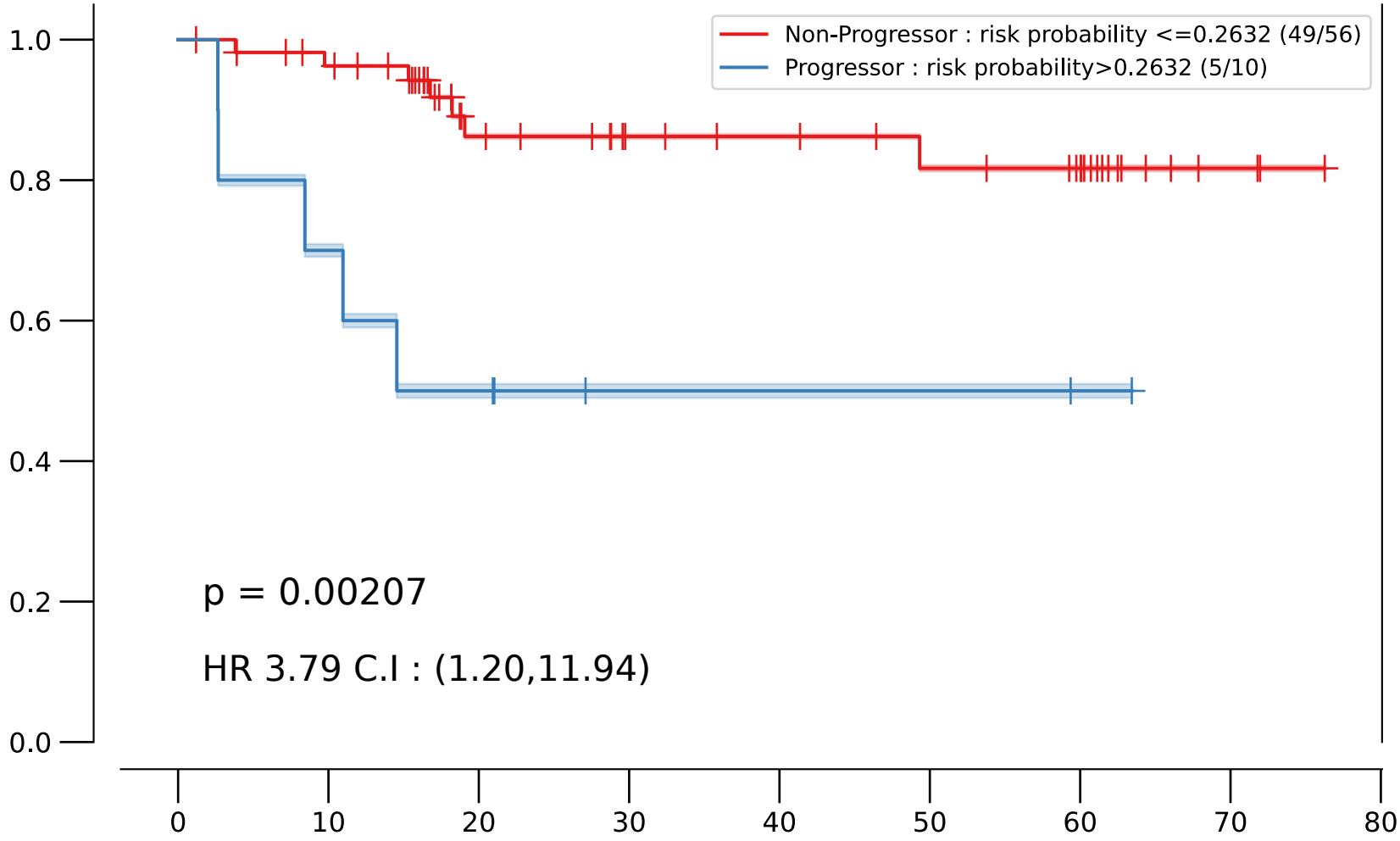

Non-Progressor : risk probability <=0.2632 (49/56)

At risk	56	50	30	23	21	18	15	3	0
Censored	0	4	20	27	29	31	34	46	49
Events	0	2	6	6	6	7	7	7	7

Progressor : risk probability>0.2632 (5/10)

At risk	10	7	5	2	2	2	1	0	0
Censored	0	0	0	3	3	3	4	5	5
Events	0	3	5	5	5	5	5	5	5

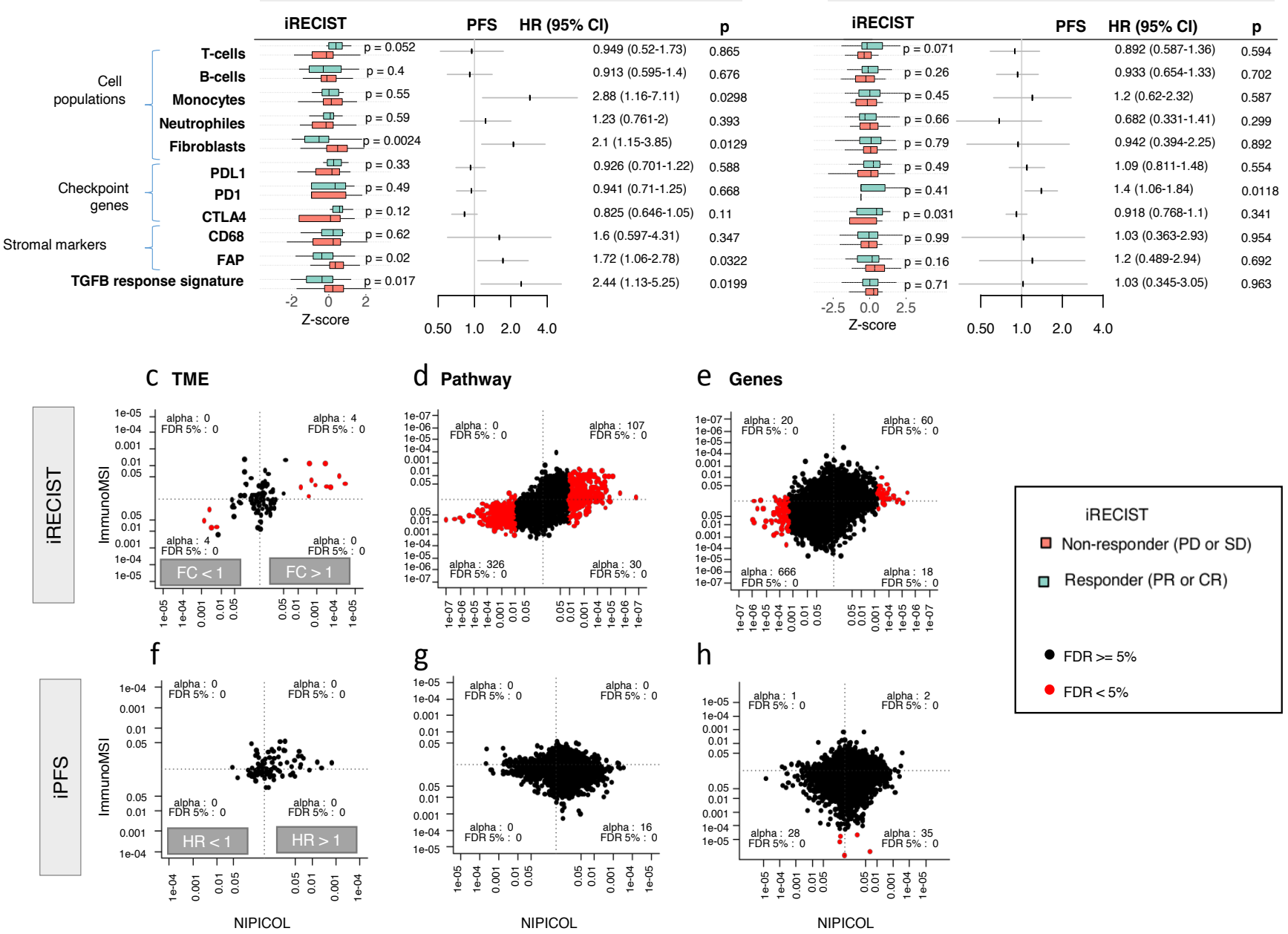
a
NIPICOL (discovery)
b
ImmunoMSI (validation)
iRECIST
PFS
HR (95% CI)
p
Cell populations
T-cells
B-cells
Monocytes
Neutrophiles
Fibroblasts
Checkpoint genes
PDL1
PD1
CTLA4
Stromal markers
CD68
FAP
TGFB response signature
p = 0.052
p = 0.4
p = 0.55
p = 0.59
p = 0.0024
p = 0.33
p = 0.49
p = 0.12
p = 0.62
p = 0.02
p = 0.017
0.949 (0.52-1.73)
0.913 (0.595-1.4)
2.88 (1.16-7.11)
1.23 (0.761-2)
2.1 (1.15-3.85)
0.926 (0.701-1.22)
0.941 (0.71-1.25)
0.825 (0.646-1.05)
1.6 (0.597-4.31)
1.72 (1.06-2.78)
2.44 (1.13-5.25)
0.865
0.676
0.0298
0.393
0.0129
0.588
0.668
0.11
0.347
0.0322
0.0199
p = 0.071
p = 0.26
p = 0.45
p = 0.66
p = 0.79
p = 0.49
p = 0.41
p = 0.031
p = 0.99
p = 0.16
p = 0.71
0.892 (0.587-1.36)
0.933 (0.654-1.33)
1.2 (0.62-2.32)
0.682 (0.331-1.41)
0.942 (0.394-2.25)
1.09 (0.811-1.48)
1.4 (1.06-1.84)
0.918 (0.768-1.1)
1.03 (0.363-2.93)
1.2 (0.489-2.94)
1.03 (0.345-3.05)
0.594
0.702
0.587
0.299
0.892
0.554
0.0118
0.341
0.954
0.692
0.963
-2 0 2
Z-score
0.50 1.0 2.0 4.0
-2.5 0.0 2.5
Z-score
0.50 1.0 2.0 4.0
c TME
d Pathway
e Genes
iRECIST
iPFS
ImmunoMSI
alpha : 0
FDR 5% : 0
alpha : 4
FDR 5% : 0
alpha : 4
FDR 5% : 0
alpha : 0
FDR 5% : 0
FC < 1
FC > 1
alpha : 0
FDR 5% : 0
alpha : 107
FDR 5% : 0
alpha : 326
FDR 5% : 0
alpha : 30
FDR 5% : 0
alpha : 20
FDR 5% : 0
alpha : 60
FDR 5% : 0
alpha : 666
FDR 5% : 0
alpha : 18
FDR 5% : 0
f
g
h
alpha : 0
FDR 5% : 0
alpha : 0
FDR 5% : 0
alpha : 0
FDR 5% : 0
alpha : 0
FDR 5% : 0
HR < 1
HR > 1
alpha : 0
FDR 5% : 0
alpha : 0
FDR 5% : 0
alpha : 16
FDR 5% : 0
alpha : 1
FDR 5% : 0
alpha : 2
FDR 5% : 0
alpha : 28
FDR 5% : 0
alpha : 35
FDR 5% : 0
NIPICOL
NIPICOL
NIPICOL
iRECIST
Non-responder (PD or SD)
Responder (PR or CR)
FDR >= 5%
FDR < 5%

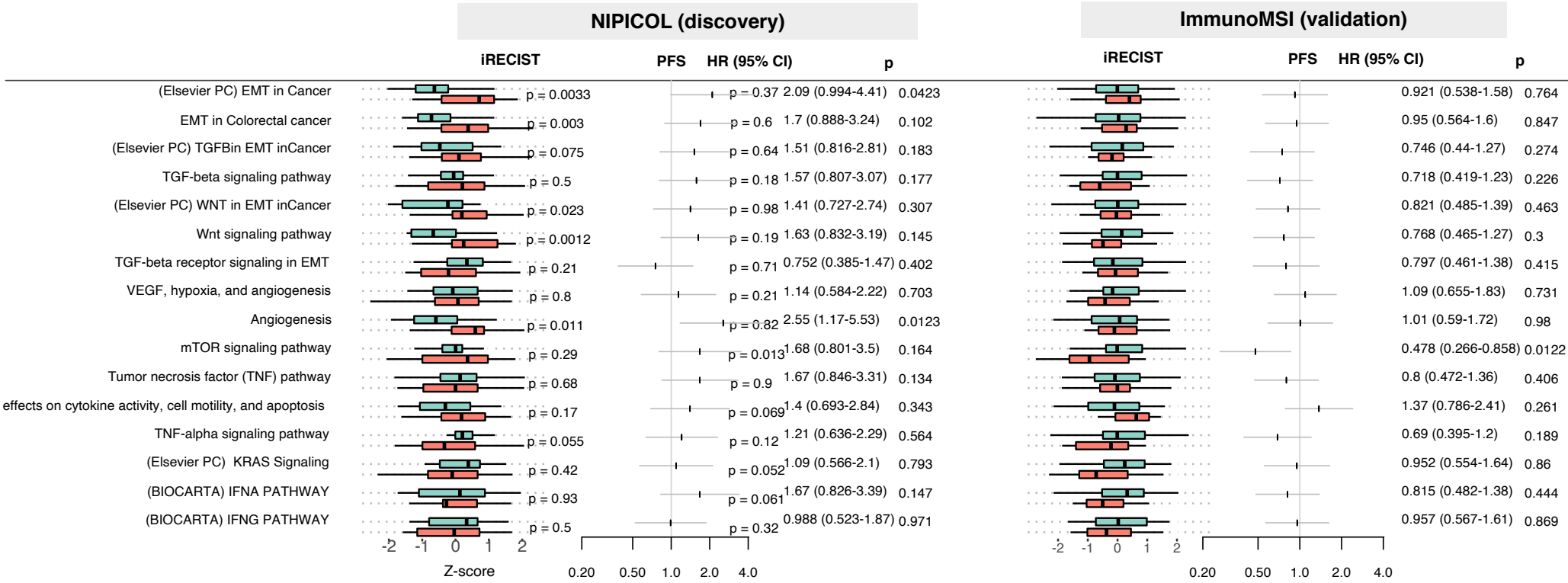
NIPICOL (discovery)
ImmunoMSI (validation)
iRECIST
PFS
HR (95% CI)
p
(Elsevier PC) EMT in Cancer
EMT in Colorectal cancer
(Elsevier PC) TGFBin EMT inCancer
TGF-beta signaling pathway
(Elsevier PC) WNT in EMT inCancer
Wnt signaling pathway
TGF-beta receptor signaling in EMT
VEGF, hypoxia, and angiogenesis
Angiogenesis
mTOR signaling pathway
Tumor necrosis factor (TNF) pathway
TNFa effects on cytokine activity, cell motility, and apoptosis
TNF-alpha signaling pathway
(Elsevier PC) KRAS Signaling
(BIOCARTA) IFNA PATHWAY
(BIOCARTA) IFNG PATHWAY
p = 0.0033
p = 0.003
p = 0.075
p = 0.5
p = 0.023
p = 0.0012
p = 0.21
p = 0.8
p = 0.011
p = 0.29
p = 0.68
p = 0.17
p = 0.055
p = 0.42
p = 0.93
p = 0.5
p = 0.37 2.09 (0.994-4.41) 0.0423
p = 0.6 1.7 (0.888-3.24) 0.102
p = 0.64 1.51 (0.816-2.81) 0.183
p = 0.18 1.57 (0.807-3.07) 0.177
p = 0.98 1.41 (0.727-2.74) 0.307
p = 0.19 1.63 (0.832-3.19) 0.145
p = 0.71 0.752 (0.385-1.47) 0.402
p = 0.21 1.14 (0.584-2.22) 0.703
p = 0.82 2.55 (1.17-5.53) 0.0123
p = 0.013 1.68 (0.801-3.5) 0.164
p = 0.9 1.67 (0.846-3.31) 0.134
p = 0.069 1.4 (0.693-2.84) 0.343
p = 0.12 1.21 (0.636-2.29) 0.564
p = 0.052 1.09 (0.566-2.1) 0.793
p = 0.061 1.67 (0.826-3.39) 0.147
p = 0.32 0.988 (0.523-1.87) 0.971
0.921 (0.538-1.58) 0.764
0.95 (0.564-1.6) 0.847
0.746 (0.44-1.27) 0.274
0.718 (0.419-1.23) 0.226
0.821 (0.485-1.39) 0.463
0.768 (0.465-1.27) 0.3
0.797 (0.461-1.38) 0.415
1.09 (0.655-1.83) 0.731
1.01 (0.59-1.72) 0.98
0.478 (0.266-0.858) 0.0122
0.8 (0.472-1.36) 0.406
1.37 (0.786-2.41) 0.261
0.69 (0.395-1.2) 0.189
0.952 (0.554-1.64) 0.86
0.815 (0.482-1.38) 0.444
0.957 (0.567-1.61) 0.869
-2 -1 0 1 2
Z-score
0.20 0.50 1.0 2.0 4.0

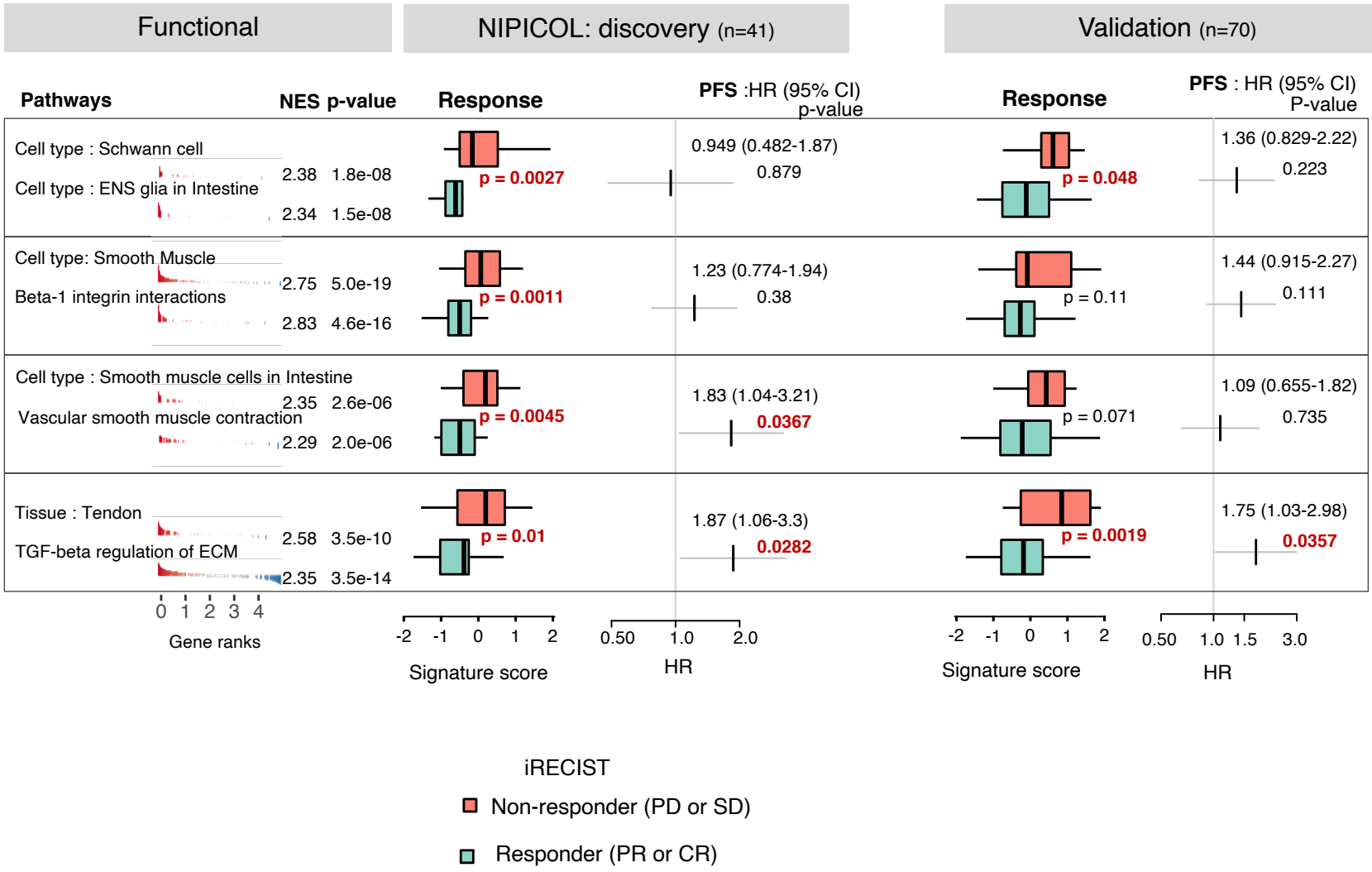
Functional
NIPICOL: discovery (n=41)
Validation (n=70)
Pathways
NES p-value
Response
PFS :HR (95% CI) p-value
Response
PFS : HR (95% CI) P-value
#1
Cell type : Schwann cell
2.38 1.8e-08
Cell type : ENS glia in Intestine
2.34 1.5e-08
p = 0.0027
0.949 (0.482-1.87)
0.879
p = 0.048
1.36 (0.829-2.22)
0.223
#2
Cell type: Smooth Muscle
2.75 5.0e-19
Beta-1 integrin interactions
2.83 4.6e-16
p = 0.0011
1.23 (0.774-1.94)
0.38
p = 0.11
1.44 (0.915-2.27)
0.111
#3
Cell type : Smooth muscle cells in Intestine
2.35 2.6e-06
Vascular smooth muscle contraction
2.29 2.0e-06
p = 0.0045
1.83 (1.04-3.21)
0.0367
p = 0.071
1.09 (0.655-1.82)
0.735
#4
Tissue : Tendon
2.58 3.5e-10
TGF-beta regulation of ECM
2.35 3.5e-14
p = 0.01
1.87 (1.06-3.3)
0.0282
p = 0.0019
1.75 (1.03-2.98)
0.0357
0 1 2 3 4
Gene ranks
-2 -1 0 1 2
Signature score
0.50 1.0 2.0
HR
-2 -1 0 1 2
Signature score
0.50 1.0 1.5 3.0
HR
iRECIST
Non-responder (PD or SD)
Responder (PR or CR)

a

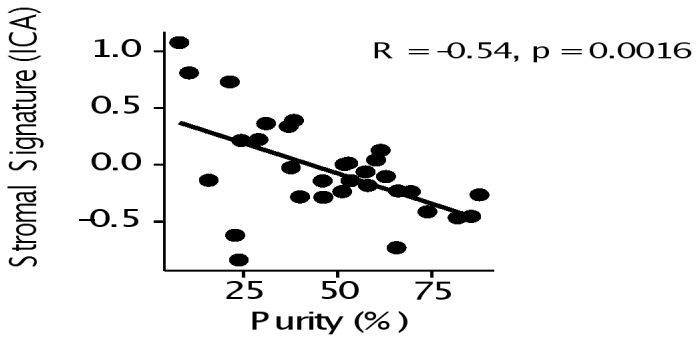
Stromal Signature (ICA)
1.0
0.5
0.0
−0.5
25
50
75
Purity (%)
R = −0.54, p = 0.0016

b

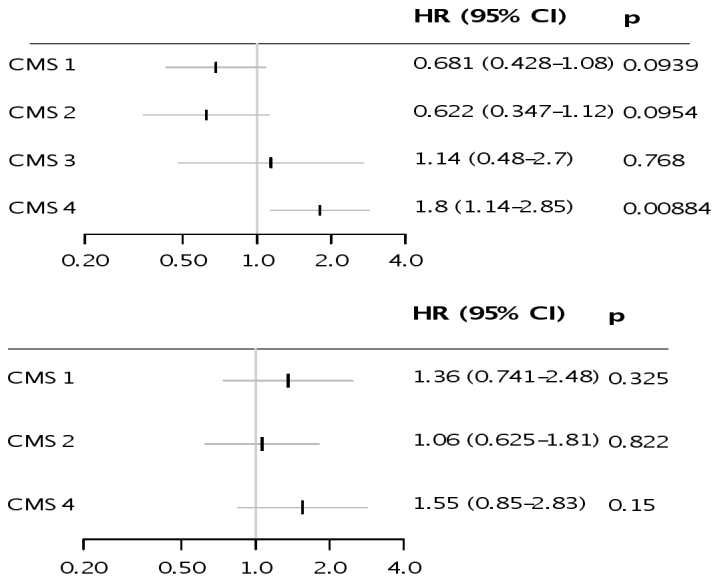
HR (95% CI)
p
CMS 1
0.681 (0.428–1.08)
0.0939
CMS 2
0.622 (0.347–1.12)
0.0954
CMS 3
1.14 (0.48–2.7)
0.768
CMS 4
1.8 (1.14–2.85)
0.00884
0.20
0.50
1.0
2.0
4.0
HR (95% CI)
p
CMS 1
1.36 (0.741–2.48)
0.325
CMS 2
1.06 (0.625–1.81)
0.822
CMS 4
1.55 (0.85–2.83)
0.15
0.20
0.50
1.0
2.0
4.0

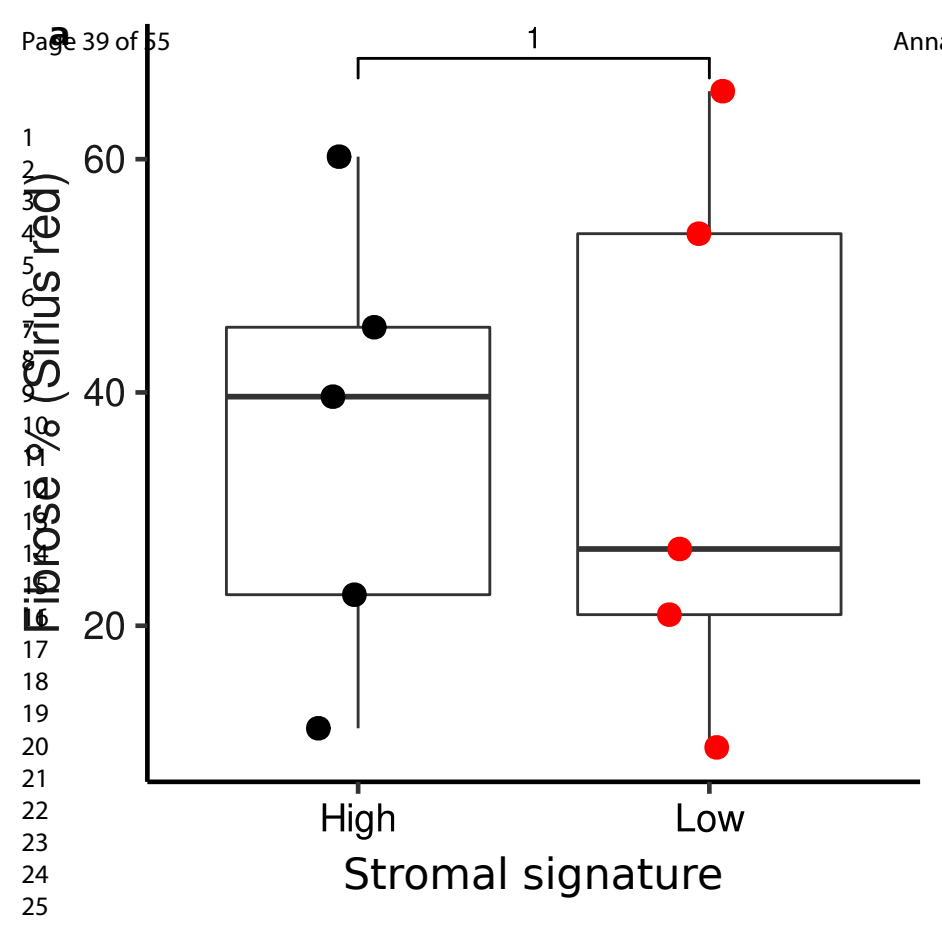

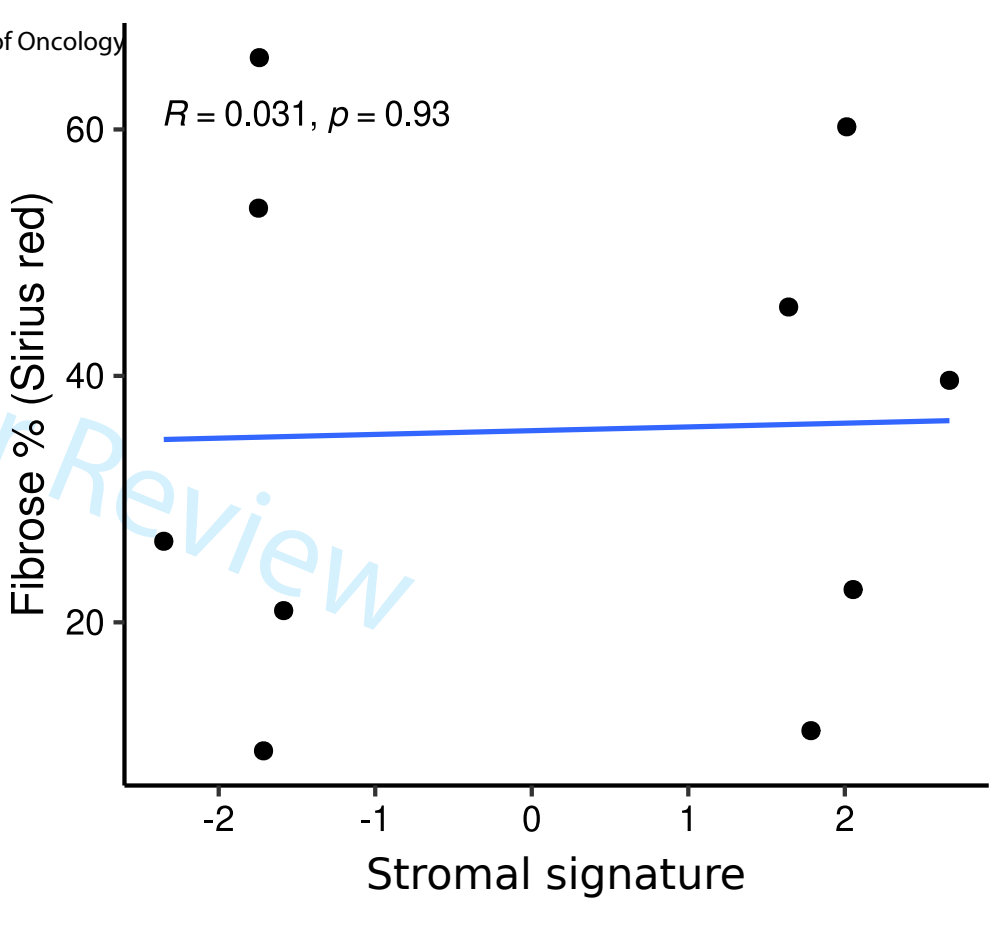

A

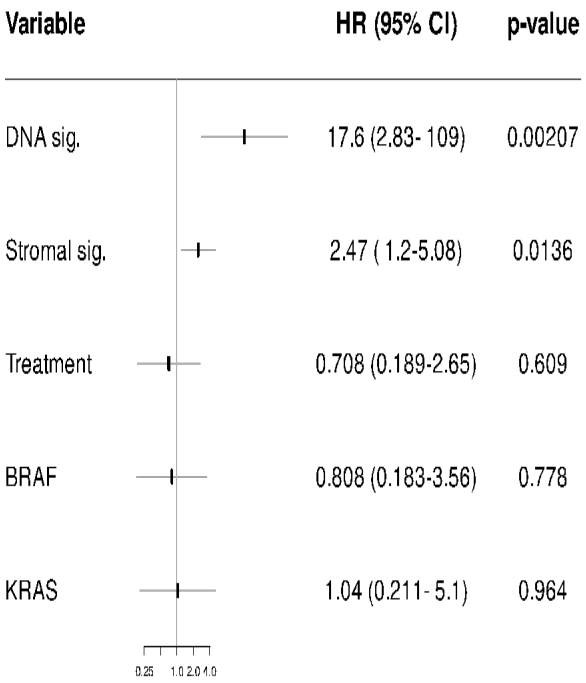
Variable
HR (95% CI)
p-value
DNA sig.
17.6 (2.83- 109)
0.00207
Stromal sig.
2.47 (1.2-5.08)
0.0136
Treatment
0.708 (0.189-2.65)
0.609
BRAF
0.808 (0.183-3.56)
0.778
KRAS
1.04 (0.211- 5.1)
0.964
0.25
1.0
2.0
4.0

B

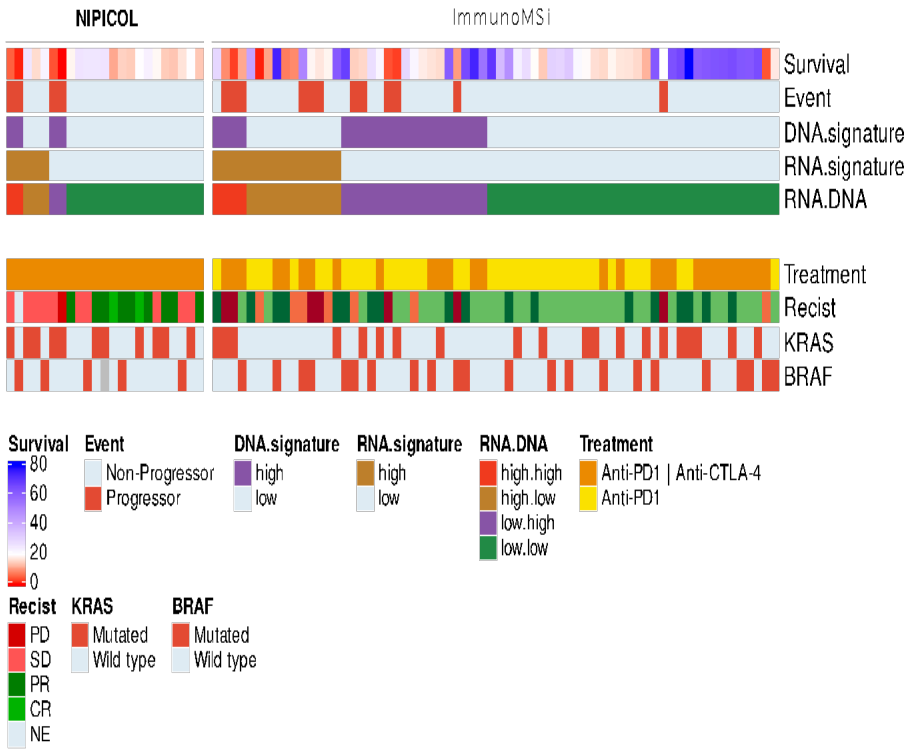
NIPICOL
ImmunoMSI
Survival
Event
DNA.signature
RNA.signature
RNA.DNA
Treatment
Recist
KRAS
BRAF
Survival
80
60
40
20
0
Event
Non-Progressor
Progressor
DNA.signature
high
low
RNA.signature
high
low
RNA.DNA
high.high
high.low
low.high
low.low
Treatment
Anti-PD1 | Anti-CTLA-4
Anti-PD1
Recist
PD
SD
PR
CR
NE
KRAS
Mutated
Wild type
BRAF
Mutated
Wild type

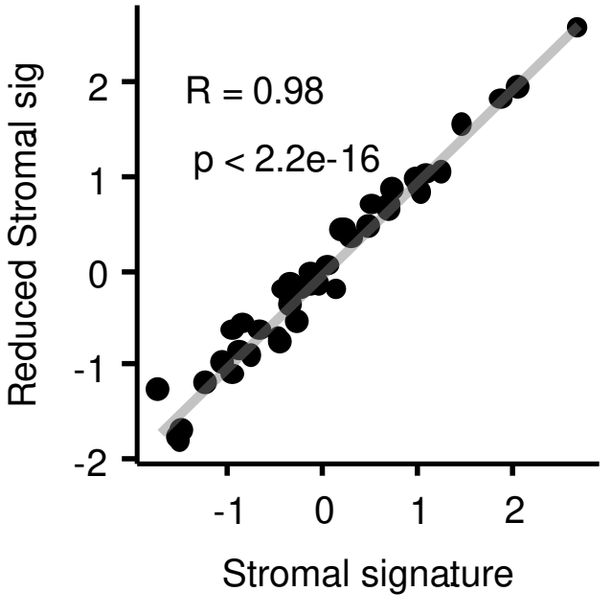

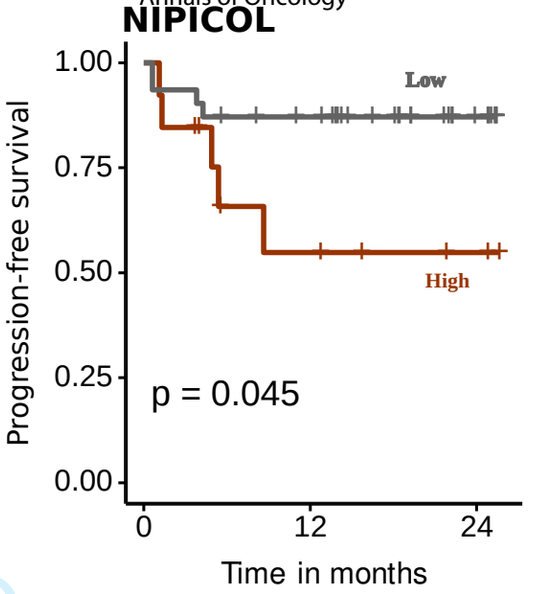

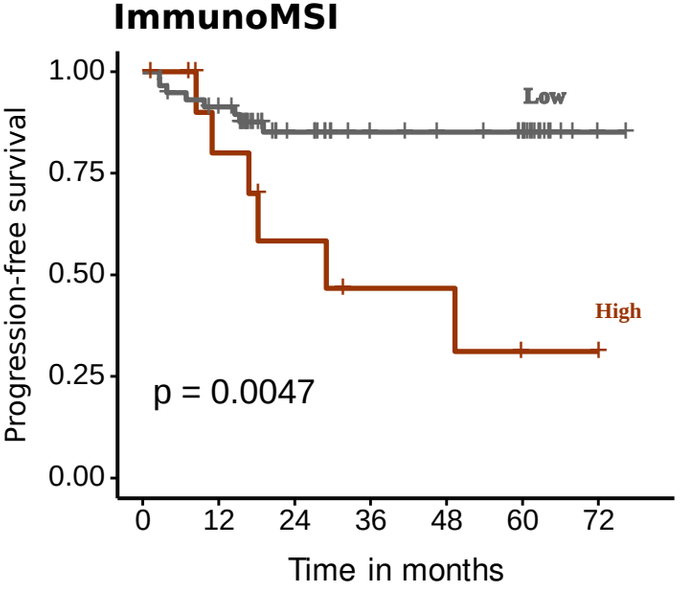

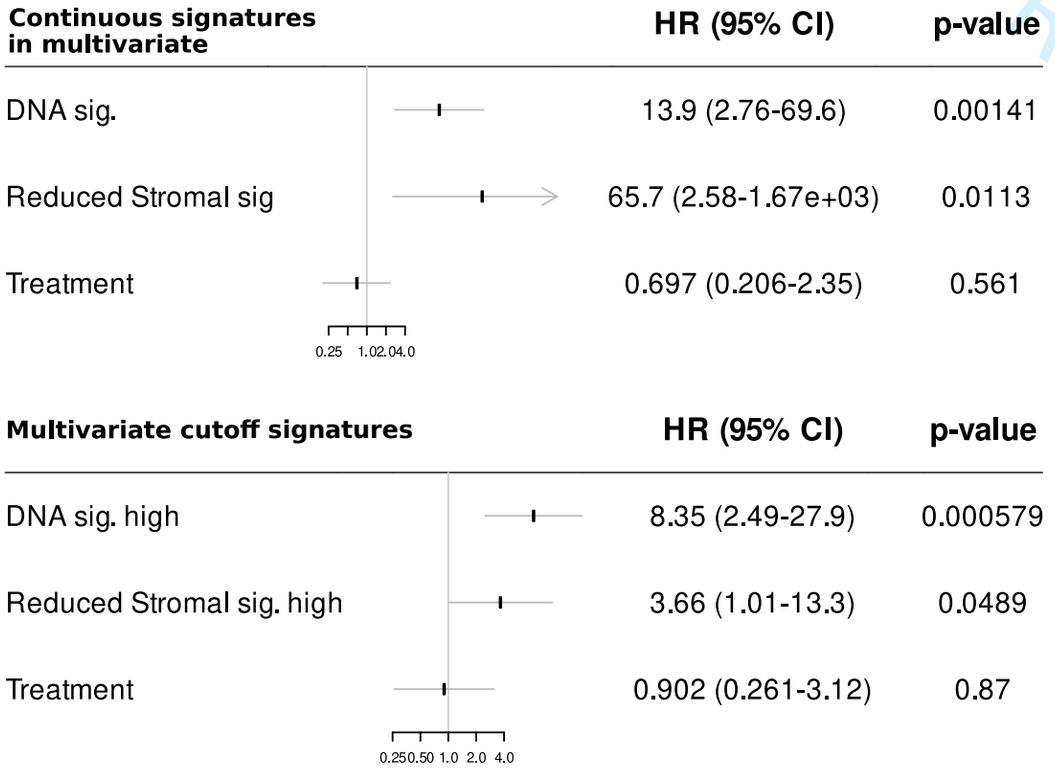

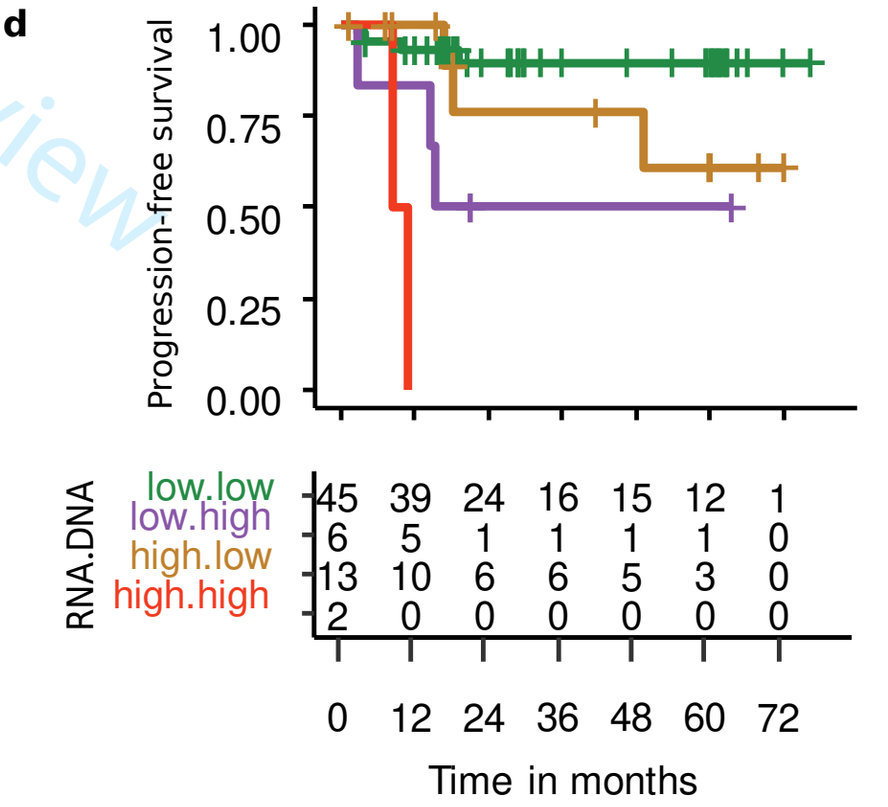

Characteristic	ImmunoMSI, N = 73[1]	Nipicol, N = 47[1]	p-value[2]
Age	59 (15)	54 (13)	0.058
Unknown	1	0	
Sex			0.87
Female	28 / 72 (39%)	19 / 47 (40%)	
Male	44 / 72 (61%)	28 / 47 (60%)	
Unknown	1	0	
ECOG performance score			0.24
≥1	36 / 71 (51%)	29 / 47 (62%)	
0	35 / 71 (49%)	18 / 47 (38%)	
Unknown	2	0	
Primary tumor location			0.49
Left colon	23 / 70 (33%)	18 / 46 (39%)	
Right colon	47 / 70 (67%)	28 / 46 (61%)	
Unknown	3	1	
BRAF			0.056
Mutated	23 / 72 (32%)	7 / 44 (16%)	
Wild type	49 / 72 (68%)	37 / 44 (84%)	
Unknown	1	3	
KRAS			0.029
Mutated	21 / 72 (29%)	23 / 47 (49%)	
Wild type	51 / 72 (71%)	24 / 47 (51%)	
Unknown	1	0	

Characteristic	**ImmunoMSI**, N = 73[1]	**Nipicol**, N = 47[1]	**p-value**[2]
NRAS			>0.99
Mutated	1 / 72 (1.4%)	1 / 43 (2.3%)	
Wild type	71 / 72 (99%)	42 / 43 (98%)	
Unknown	1	4	
Origin of MMR deficiency			0.82
Known germline mutation	20 / 30 (67%)	27 / 39 (69%)	
Sporadic	10 / 30 (33%)	12 / 39 (31%)	
Unknown	43	8	
Surgery of the primary tumor	71 / 72 (99%)	43 / 44 (98%)	>0.99
Unknown	1	3	
Number of metastatic sites			0.50
1	27 / 72 (38%)	14 / 47 (30%)	
2	26 / 72 (36%)	18 / 47 (38%)	
3	13 / 72 (18%)	10 / 47 (21%)	
4	6 / 72 (8.3%)	3 / 47 (6.4%)	
5	0 / 72 (0%)	2 / 47 (4.3%)	
Unknown	1	0	
Number of prior lines			0.006
0	9 / 72 (12%)	0 / 47 (0%)	
1	21 / 72 (29%)	8 / 47 (17%)	
2	32 / 72 (44%)	22 / 47 (47%)	
3	8 / 72 (11%)	12 / 47 (26%)	

Characteristic	**ImmunoMSI**, N = 73[1]	**Nipicol**, N = 47[1]	**p-value**[2]
4	1 / 72 (1.4%)	3 / 47 (6.4%)	
5	1 / 72 (1.4%)	2 / 47 (4.3%)	
Unknown	1	0	
Type of immunotherapy			<0.001
Anti-PD1	43 / 72 (60%)	0 / 47 (0%)	
Anti-PD1 | Anti-CTLA-4	29 / 72 (40%)	47 / 47 (100%)	
Unknown	1	0	
iRECIST			<0.001
CR	20 / 70 (29%)	2 / 44 (4.5%)	
PD	8 / 70 (11%)	3 / 44 (6.8%)	
PR	35 / 70 (50%)	15 / 44 (34%)	
SD	7 / 70 (10%)	24 / 44 (55%)	
Unknown	3	3	
Status			0.058
MSI	73 / 73 (100%)	44 / 47 (94%)	
MSS	0 / 73 (0%)	3 / 47 (6.4%)	

[1] Mean (SD); n / N (%)

[2] Wilcoxon rank sum test; Pearson's Chi-squared test; Fisher's exact test

ID	Cohort	Age	Sex	Status	DNA	RNA	Drug	Response	PFS	Event
IMSI_0150	Nipicol	50	Female	MSI	Exome	RNAseq	Anti-PD1	SD	25.29774	0
IMSI_0153	Nipicol	54	Male	MSI	Exome	RNAseq	Anti-PD1	PR	25.62628	0
IMSI_0188	Nipicol	49	Male	MSI	NA	RNAseq	Anti-PD1	PR	25.3963	0
IMSI_0195	Nipicol	39	Male	MSI	NA	RNAseq	Anti-PD1	PR	24.83778	0
IMSI_0181	Nipicol	64	Female	MSI	NA	RNAseq	Anti-PD1	SD	5.519507	0
IMSI_0187	Nipicol	38	Male	MSI	NA	RNAseq	Anti-PD1	SD	25.42916	0
IMSI_0180	Nipicol	58	Female	MSI	NA	RNAseq	Anti-PD1	SD	5.552361	0
IMSI_0151	Nipicol	32	Male	MSI	Exome	RNAseq	Anti-PD1	SD	25.03491	0
IMSI_0152	Nipicol	39	Male	MSI	Exome	RNAseq	Anti-PD1	PR	24.80493	0
IMSI_0179	Nipicol	60	Female	MSI	NA	RNAseq	Anti-PD1	SD	23.85216	0
IMSI_0146	Nipicol	63	Female	MSI	Exome	RNAseq	Anti-PD1	SD	24.80493	0
IMSI_0159	Nipicol	66	Male	MSI	NA	RNAseq	Anti-PD1	SD	8.640657	1
IMSI_0155	Nipicol	52	Male	MSI	Exome	RNAseq	Anti-PD1	SD	21.8152	0
IMSI_0189	Nipicol	63	Female	MSI	NA	RNAseq	Anti-PD1	SD	21.97947	0
IMSI_0154	Nipicol	49	Male	MSI	Exome	RNAseq	Anti-PD1	CR	10.97331	0
IMSI_0163	Nipicol	57	Female	MSI	Exome	RNAseq	Anti-PD1	SD	4.895277	1
IMSI_0156	Nipicol	63	Male	MSI	Exome	RNAseq	Anti-PD1	PR	14.68583	0
IMSI_0173	Nipicol	68	Male	MSI	NA	RNAseq	Anti-PD1	SD	21.61807	0
IMSI_0160	Nipicol	65	Male	MSI	Exome	RNAseq	Anti-PD1	SD	3.811088	1
IMSI_0165	Nipicol	54	Female	MSI	Exome	RNAseq	Anti-PD1	PR	22.20945	0
IMSI_0190	Nipicol	46	Male	MSI	NA	RNAseq	Anti-PD1	SD	22.2423	0
IMSI_0191	Nipicol	65	Male	MSI	NA	RNAseq	Anti-PD1	PR	13.96304	0
IMSI_0158	Nipicol	58	Female	MSI	Exome	RNAseq	Anti-PD1	PR	14.22587	0
IMSI_0194	Nipicol	72	Male	MSI	NA	RNAseq	Anti-PD1	PR	4.271047	1
IMSI_0175	Nipicol	44	Male	MSI	Exome	RNAseq	Anti-PD1	SD	19.25257	0
IMSI_0147	Nipicol	22	Male	MSI	Exome	RNAseq	Anti-PD1	SD	15.70431	0
IMSI_0162	Nipicol	66	Male	MSI	Exome	RNAseq	Anti-PD1	CR	19.21971	0
IMSI_0185	Nipicol	32	Male	MSI	Exome	RNAseq	Anti-PD1	#N/A	1.314168	1
IMSI_0161	Nipicol	50	Male	MSI	NA	RNAseq	Anti-PD1	SD	8.082136	0
IMSI_0148	Nipicol	31	Male	MSI	Exome	RNAseq	Anti-PD1	PR	18.06982	0
IMSI_0186	Nipicol	36	Male	MSI	Exome	RNAseq	Anti-PD1	PR	13.83162	0
IMSI_0184	Nipicol	36	Female	MSI	NA	RNAseq	Anti-PD1	#N/A	0.62423	1
IMSI_0169	Nipicol	33	Male	MSI	NA	RNAseq	Anti-PD1	PR	12.81314	0
IMSI_0167	Nipicol	61	Male	MSI	Exome	RNAseq	Anti-PD1	SD	18.3655	0
IMSI_0177	Nipicol	59	Female	MSI	NA	RNAseq	Anti-PD1	#N/A	1.117043	1
IMSI_0193	Nipicol	59	Male	MSI	NA	RNAseq	Anti-PD1	SD	18.43121	0
IMSI_0171	Nipicol	69	Male	MSI	NA	RNAseq	Anti-PD1	SD	3.679671	0
IMSI_0164	Nipicol	62	Female	MSI	Exome	RNAseq	Anti-PD1	PD	0.62423	1
IMSI_0178	Nipicol	76	Female	MSI	NA	RNAseq	Anti-PD1	SD	12.74743	0
IMSI_0166	Nipicol	61	Female	MSI	NA	RNAseq	Anti-PD1	SD	3.975359	0
IMSI_0192	Nipicol	37	Male	MSI	NA	RNAseq	Anti-PD1	SD	5.38809	1
IMSI_0172	Nipicol	56	Male	MSI	Exome	RNAseq	Anti-PD1	SD	16.45996	0
IMSI_0170	Nipicol	64	Female	MSI	Exome	RNAseq	Anti-PD1	PR	13.60164	0
IMSI_0168	Nipicol	77	Female	MSI	Exome	RNAseq	Anti-PD1	PR	14.22587	0
IMSI_0149	Nipicol	65	Female	MSS	Exome	RNAseq	Anti-PD1	PD	2.529774	1
IMSI_0157	Nipicol	51	Female	MSS	Exome	RNAseq	Anti-PD1	PD	4.13963	1
IMSI_0183	Nipicol	52	Female	MSS	Exome	RNAseq	Anti-PD1	PR	13.53593	0
RICKI-070T	ImmunoM	82	Female	MSI	Targeted S	RNAseq	Anti-PD1	PR	59.26667	0
RICKI-053T	ImmunoM	43	Male	MSI	Targeted S	RNAseq	Anti-PD1	CR	59.36667	0
RICKI-060T	ImmunoM	52	Male	MSI	Targeted S	RNAseq	Anti-PD1	PD	2.666667	1
RICKI-001T	ImmunoM	73	Male	MSI	Targeted S	RNAseq	Anti-PD1	CR	66.03333	0
RICKI-054T	ImmunoM	79	Male	MSI	Targeted S	RNAseq	Anti-PD1	PR	61.87097	0
RICKI-009T	ImmunoM	89	Female	MSI	Targeted S	RNAseq	Anti-PD1	PR	22.77419	0
RICKI-071T	ImmunoM	60	Male	MSI	Targeted S	RNAseq	Anti-PD1	CR	60.26667	0
RICKI-008T	ImmunoM	34	Male	MSI	Targeted S	RNAseq	Anti-PD1	CR	46.43333	0
RICKI-064T	ImmunoM	74	Male	MSI	Targeted S	RNAseq	Anti-PD1	PD	16.76667	1
RICKI-072T	ImmunoM	66	Male	MSI	Targeted S	RNAseq	Anti-PD1	SD	18.17857	0
RICKI-055T	ImmunoM	69	Female	MSI	Targeted S	RNAseq	Anti-PD1	SD	49.32258	1
RICKI-002T	ImmunoM	64	Female	MSI	Targeted S	RNAseq	Anti-PD1	PD	29	1
RICKI-073T	ImmunoM	48	Male	MSI	Targeted S	RNAseq	Anti-PD1	PR	61.13333	0
RICKI-065T	ImmunoM	64	Female	MSI	Targeted S	RNAseq	Anti-PD1	CR	64.36667	0
RICKI-066T	ImmunoM	65	Male	MSI	Targeted S	RNAseq	Anti-PD1	CR	76.26667	0
RICKI-074T	ImmunoM	64	Female	MSI	Targeted S	RNAseq	Anti-PD1	PR	71.8	0
RICKI-067T	ImmunoM	34	Male	MSI	Targeted S	RNAseq	Anti-PD1	CR	63.43333	0
RICKI-075T	ImmunoM	47	Female	MSI	Targeted S	RNAseq	Anti-PD1	PR	61.46667	0
RICKI-048T	ImmunoM	61	Male	MSI	Targeted S	RNAseq	Anti-PD1	PD	19.06451	1
RICKI-069T	ImmunoM	55	Male	MSI	Targeted S	RNAseq	Anti-PD1	CR	64.06667	0
RICKI-076T	ImmunoM	35	Female	MSI	Targeted S	RNAseq	Anti-PD1	CR	62.74194	0
RICKI-062T	ImmunoM	50	Male	MSI	Targeted S	RNAseq	Anti-PD1	PD	9.741935	1
RICKI-077T	ImmunoM	65	Female	MSI	Targeted S	RNAseq	Anti-PD1	PR	10.96667	1
RICKI-049T	ImmunoM	77	Female	MSI	Targeted S	RNAseq	Anti-PD1	CR	71.96774	0
RICKI-078T	ImmunoM	26	Male	MSI	Targeted S	RNAseq	Anti-PD1	PR	60.70968	0
RICKI-046T	ImmunoM	60	Male	MSI	Targeted S	RNAseq	Anti-PD1	CR	60.03333	0
RICKI-079T	ImmunoM	49	Male	MSI	Targeted S	RNAseq	Anti-PD1	CR	59.74194	0
RICKI-080T	ImmunoM	53	Male	MSI	Targeted S	RNAseq	Anti-PD1	PR	60.06667	0
RICKI-081T	ImmunoM	59	Male	MSI	Targeted S	RNAseq	Anti-PD1	PR	53.77419	0
RICKI-082T	ImmunoM	58	Male	MSI	Targeted S	RNAseq	Anti-PD1	PR	62.5	0
RICKI-005T	ImmunoM	33	Male	MSI	Targeted S	RNAseq	Anti-PD1	CR	41.36667	0
RICKI-006T	ImmunoM	45	Female	MSI	Targeted S	RNAseq	Anti-PD1	PR	35.83333	0
RICKI-026T	ImmunoM	62	Male	MSI	Targeted S	RNAseq	Anti-PD1	PR	32.4	0
RICKI-007T	ImmunoM	74	Female	MSI	Targeted S	RNAseq	Anti-PD1	SD	14.54839	1
RICKI-003T	ImmunoM	70	Male	MSI	Targeted S	RNAseq	Anti-PD1	PR	67.86667	0
RICKI-061T	ImmunoM	77	Male	MSI	Targeted S	RNAseq	Anti-PD1	PD	18.22581	1
RICKI-017T	ImmunoM	55	Female	MSI	Targeted S	RNAseq	Anti-PD1	PR	31.6	0
RICKI-016T	ImmunoM	50	Male	MSI	Targeted S	RNAseq	Anti-PD1	PR	29.73333	0
RICKI-025T	ImmunoM	63	Female	MSI	Targeted S	RNAseq	Anti-PD1	PR	28.73333	0
RICKI-018T	ImmunoM	67	Male	MSI	Targeted S	RNAseq	Anti-PD1	PR	29.56667	0
RICKI-022T	ImmunoM	65	Female	MSI	Targeted S	RNAseq	Anti-PD1	PR	2.642857	1
RICKI-023T	ImmunoM	61	Female	MSI	Targeted S	RNAseq	Anti-PD1	CR	28.8	0
RICKI-024T	ImmunoM	72	Male	MSI	Targeted S	RNAseq	Anti-PD1	CR	27.2	0
RICKI-011T	ImmunoM	51	Male	MSI	Targeted S	RNAseq	Anti-PD1	PR	27.53333	0
RICKI-019T	ImmunoM	48	Male	MSI	Targeted S	RNAseq	Anti-PD1	CR	27.1	0
RICKI-021T	ImmunoM	59	Female	MSI	Targeted S	RNAseq	Anti-PD1	PD	3.806452	1
RICKI-028T	ImmunoM	52	Male	MSI	Targeted S	RNAseq	Anti-PD1	SD	21.03333	0
RICKI-020T	ImmunoM	72	Male	MSI	Targeted S	RNAseq	Anti-PD1	CR	20.93333	0
RICKI-029T	ImmunoM	37	Male	MSI	Targeted S	RNAseq	Anti-PD1	PR	20.46667	0
RICKI-012T	ImmunoM	78	Male	MSI	Targeted S	RNAseq	Anti-PD1	PR	15.32258	1
RICKI-013T	ImmunoM	67	Female	MSI	Targeted S	RNAseq	Anti-PD1	CR	18.83333	0
RICKI-084T	ImmunoM	70	Female	MSI	Targeted S	RNAseq	Anti-PD1	PR	17.06667	0
RICKI-031T	ImmunoM	62	Male	MSI	Targeted S	RNAseq	Anti-PD1	PR	18.73333	0
RICKI-037T	ImmunoM	57	Male	MSI	Targeted S	RNAseq	Anti-PD1	PR	18.16667	0
RICKI-038T	ImmunoM	59	Male	MSI	Targeted S	RNAseq	Anti-PD1	PR	17.36667	0
RICKI-039T	ImmunoM	33	Male	MSI	Targeted S	RNAseq	Anti-PD1	PR	16.6	0
RICKI-014T	ImmunoM	61	Female	MSI	Targeted S	RNAseq	Anti-PD1	SD	1.193548	0
RICKI-040T	ImmunoM	28	Male	MSI	Targeted S	RNAseq	Anti-PD1	CR	16.36667	0
RICKI-041T	ImmunoM	61	Female	MSI	Targeted S	RNAseq	Anti-PD1	PR	16.33333	0
RICKI-033T	ImmunoM	78	Female	MSI	Targeted S	RNAseq	Anti-PD1	PR	16.03226	0
RICKI-042T	ImmunoM	65	Female	MSI	Targeted S	RNAseq	Anti-PD1	PR	15.76667	0
RICKI-043T	ImmunoM	75	Male	MSI	Targeted S	RNAseq	Anti-PD1	PR	15.56667	0
RICKI-035T	ImmunoM	58	Female	MSI	Targeted S	RNAseq	Anti-PD1	PR	15.36667	0
RICKI-045T	ImmunoM	58	Female	MSI	Targeted S	RNAseq	Anti-PD1	PD	8.433333	1
RICKI-044T	ImmunoM	43	Male	MSI	Targeted S	RNAseq	Anti-PD1	PR	11.93333	0
RICKI-015T	ImmunoM	83	Female	MSI	Targeted S	RNAseq	Anti-PD1	PR	13.96667	0
RICKI-030T	ImmunoM	36	Male	MSI	Targeted S	RNAseq	Anti-PD1	#N/A	6.866667	1
RICKI-032T	ImmunoM	40	Male	MSI	Targeted S	RNAseq	Anti-PD1	PR	10.4	0
RICKI-051T	ImmunoM	27	Male	MSI	Targeted S	RNAseq	Anti-PD1	SD	8.266667	0
RICKI-050T	ImmunoM	72	Female	MSI	Targeted S	RNAseq	Anti-PD1	CR	7.16129	0
RICKI-083T	ImmunoM	70	Male	MSI	Targeted S	RNAseq	Anti-PD1	SD	3.9	0
RICKI-059T	ImmunoM	78	Female	MSI	Targeted S	RNAseq	Anti-PD1	#N/A	#N/A	#N/A

ENSid	Symbol	weight
ENSG000001(	FNDC1	5.10420386
ENSG000001(	SFRP2	4.30791092
ENSG000001(	COMP	4.08019176
ENSG000001:	AOC3	4.06685237
ENSG000001:	EFEMP1	3.78175791
ENSG000001(	MOGAT2	-3.7740728
ENSG000001(	SFRP4	3.71450879
ENSG000001(	MEDAG	3.68321604
ENSG000002(	HNF1A-AS1	-3.6323767
ENSG000001:	LRRC15	3.58531426
ENSG000001(	SYNC	3.55970288
ENSG000001(	IHH	-3.4818844
ENSG000002:	AC103702.2	-3.4495976
ENSG000002:	MIR194-2HG	-3.4477355
ENSG000001(	CHP2	-3.4388336
ENSG000001:	STEAP4	3.42856296
ENSG000001:	OPLAH	-3.4139494
ENSG000001(	MYO1A	-3.3420832
ENSG000001:	SSC5D	3.32262723
ENSG000001(	DPT	3.28461284
ENSG000001(	ESPN	-3.2834087
ENSG000001(	DMBT1	-3.2508707
ENSG000001(	MFAP5	3.20264084
ENSG000001(	JCAD	3.17143233
ENSG000001(	LHFPL6	3.1522329
ENSG000002(	NEU4	-3.1504617
ENSG000002(	AC132217.1	3.14969389
ENSG000001(	CYP4F12	-3.1448367
ENSG000001(	UCHL1	3.12997833
ENSG000001:	GPR35	-3.1268892
ENSG000002:	AL355987.4	-3.1196924
ENSG000001:	GFPT2	3.1067951
ENSG000001(	ASPN	3.09936507
ENSG000000(	YBX2	-3.0951517
ENSG000001(	MOGAT3	-3.0917462
ENSG000001(	FGF7	3.05626741
ENSG000002:	LIX1L	3.05311432
ENSG000002(	AC104083.1	3.04291511
ENSG000001:	MMP19	3.02492672
ENSG000000:	IGF1	2.98795178
ENSG000001:	COL10A1	2.98713455
ENSG000001(	ITGBL1	2.98659956
ENSG000001(	SLIT3	2.96293964
ENSG000001(	ECM2	2.9601298
ENSG000000:	DPEP1	-2.9377308
ENSG000001:	TMTC1	2.93355859
ENSG000001(	EMCN	2.90272468
ENSG000001:	KIF12	-2.8889434
ENSG000000:	SLC6A7	-2.8810662
ENSG000001:	CYP2J2	-2.8798694
ENSG000002:	GAS6-AS1	-2.8775443
ENSG000001(	CYR61	2.85765177
ENSG000001:	TSPAN2	2.85740009
ENSG000000:	GUCY2C	-2.8539231
ENSG000001(	CPED1	2.83495762
ENSG000001(	RSPH1	-2.8306275
ENSG000002:	TENM3	2.80218401
ENSG000001(	MFAP4	2.80097456
ENSG000000(	EML1	2.78458682
ENSG000001(	LMOD1	2.78009958
ENSG000001:	PDZRN3	2.77048747
ENSG000001(	FABP1	-2.7664399
ENSG000001:	LUM	2.76330963
ENSG000001:	CES3	-2.742092
ENSG000001(	DEGS2	-2.7379178
ENSG000001(	CXCL12	2.73735607
ENSG000001:	MGP	2.72643546
ENSG000001(	TNFRSF11A	-2.7234544
ENSG000000(	HSPB6	2.72059127
ENSG000001:	ZNF296	-2.7164563
ENSG000001(	PIGR	-2.7153683
ENSG000001:	DDC	-2.7066467
ENSG000001!	COLEC12	2.70112862
ENSG000001(	ROR2	2.69878886
ENSG000000(	CEACAM7	-2.6957512
ENSG000001:	DUSP1	2.69013069
ENSG000001:	KLRD1	2.68498717
ENSG000001:	HOXB9	-2.6743332
ENSG000001(	OLFM4	-2.6683462
ENSG000001(	GGT6	-2.6586474
ENSG000001:	PPP1R1B	-2.6554224
ENSG000001(	CCNF	-2.6542216
ENSG000001:	REEP6	-2.6406269
ENSG000001:	RUNX2	2.63767694
ENSG000002(	RNU6-1327P	-2.6359727
ENSG000001(	MYO7B	-2.6349204
ENSG000000:	LXN	2.63219126
ENSG000001(	BDH1	-2.6320779
ENSG000000(	PRKCZ	-2.630177
ENSG000000(	PLA2G10	-2.6272585
ENSG000001(	CRISPLD2	2.62520801
ENSG000001!	SH3RF2	-2.6199242
ENSG000001:	CPXM2	2.61602843
ENSG000001(	A1CF	-2.6055727
ENSG000001!	SULT1C2	-2.5911941
ENSG000002(	SPIRE2	-2.5842921
ENSG000001(	OSMR	2.57883696
ENSG000001:	ANKS4B	-2.575791
ENSG000001(	SLC6A20	-2.5589211
ENSG000001(	TMEM102	-2.5543287
ENSG000001:	HSD11B2	-2.5508296
ENSG000000(	CFTR	-2.5507324
ENSG000001(	EVPL	-2.5478452
ENSG000002(	RN7SL559P	-2.5380794
ENSG000000(	CCDC80	2.5284954
ENSG000001:	CPNE7	-2.5164189
ENSG000001:	TGFB3	2.51263919
ENSG000001:	A4GALT	2.51250406
ENSG000002(	VGLL3	2.51228151
ENSG000001:	RAB17	-2.5109126
ENSG000000!	PRSS8	-2.5103548
ENSG000001(	COX7A1	2.50918775
ENSG000000(	COPZ2	2.48249964
ENSG000001:	CNN1	2.47735125
ENSG000001:	CSMD2	2.47498771
ENSG000001!	RHPN1	-2.4675944
ENSG000001:	CYP1B1	2.45603284
ENSG000002:	AC009133.1	-2.4556284
ENSG000002(	STON1	2.453239
ENSG000001(	FAM193B	-2.4480303
ENSG000001:	CDH5	2.44664277
ENSG000000!	ENTPD2	-2.4464431
ENSG000002:	TNFSF12	2.4331992
ENSG000001(	RNF43	-2.4330871
ENSG000001:	BNC2	2.43236701
ENSG000001!	TMEM45B	-2.426239
ENSG000002:	LINC00623	2.42512842
ENSG000001(	BOC	2.42172423
ENSG000001:	TWIST1	2.42116864

ENSG000002	CKMT1B	-2.4209972
ENSG000001	CACNA2D1	2.41522808
ENSG000000	PALM	2.40028821
ENSG000000	FAP	2.39438999
ENSG000000	COL16A1	2.39200067
ENSG000001	ADH1B	2.38962734
ENSG000000	MLXIPL	-2.3874269
ENSG000001	TNFAIP6	2.36927496
ENSG000001	FBLN5	2.36748176
ENSG000001	PRELP	2.36044837
ENSG000001	NOXO1	-2.3592309
ENSG000001	GIPC2	-2.3565795
ENSG000001	AZGP1	-2.3552531
ENSG000001	SAA1	2.35490426
ENSG000001	ANGPTL2	2.35244276
ENSG000000	STOML1	2.34418928
ENSG000001	SLC29A2	-2.341757
ENSG000002	BTBD19	2.33572824
ENSG000002	AC087388.1	-2.3264506
ENSG000001	LOX	2.32580601
ENSG000001	ZDHHC23	-2.3129355
ENSG000001	PLAC9	2.31118575
ENSG000001	ATP6V1C2	-2.3084971
ENSG000001	CSRNP1	2.30573514
ENSG000002	C14orf132	2.30110158
ENSG000001	LRP4	-2.2972655
ENSG000001	GUCY1A3	2.29672717
ENSG000001	THBS2	2.29125828
ENSG000002	DHRS11	-2.2839635
ENSG000001	INCENP	-2.2834472
ENSG000001	ASCL2	-2.2830566
ENSG000001	RNF144B	2.27886073
ENSG000000	SEMA4G	-2.2785769
ENSG000001	SGPP2	-2.271301
ENSG000002	CPT1B	-2.2649018
ENSG000001	SPC25	-2.250969
ENSG000002	PHGR1	-2.2496352
ENSG000001	C1orf162	2.2469563
ENSG000002	MYO15B	-2.2407008
ENSG000001	ALDOB	-2.2399809
ENSG000001	MYB	-2.2368562
ENSG000001	PBLD	-2.2335698
ENSG000000	CDHR5	-2.2334101
ENSG000002	DNM3OS	2.23185767
ENSG000000	FKBP7	2.23117643
ENSG000001	ANO9	-2.2302804
ENSG000000	PARP3	-2.2300918
ENSG000000	SULT2B1	-2.2262162
ENSG000001	AGMAT	-2.2254478
ENSG000001	HMGCS2	-2.2204418
ENSG000001	MEIS1	2.21438371
ENSG000001	CTGF	2.21025359
ENSG000001	PODNL1	2.21002783
ENSG000001	PDE10A	2.20695482
ENSG000002	LINC02086	-2.1984313
ENSG000000	IYD	-2.1955679
ENSG000001	PIEZO2	2.18800181
ENSG000001	TROAP	-2.1856571
ENSG000000	FBLN1	2.17547884
ENSG000001	C2orf82	-2.1711947
ENSG000001	RGMA	2.16953268
ENSG000001	OLFML2B	2.16885593
ENSG000001	GPC6	2.1653184
ENSG000002	AC018638.8	-2.1637824
ENSG000001	GLI3	2.16142102
ENSG000001	AMIGO2	2.15670404
ENSG000001	GPR78	2.15374608
ENSG000001	SSPN	2.15338107
ENSG000001	CTSK	2.15312225
ENSG000000	KCNQ1	-2.1526444
ENSG000000	ADAMTS2	2.15083602
ENSG000001	GDPD3	-2.150816
ENSG000001	CCSER1	-2.1499834
ENSG000001	PDSS1	-2.1449331
ENSG000001	CCL2	2.14424312
ENSG000000	FGR	2.14105989
ENSG000002	AC093840.1	-2.1362235
ENSG000001	DQX1	-2.1314835
ENSG000001	SELPLG	2.13018363
ENSG000001	VIPR1	-2.1300905
ENSG000001	ANPEP	-2.1287041
ENSG000002	AC018629.1	-2.1201524
ENSG000001	LCN2	-2.1194597
ENSG000001	C10orf10	2.11917274
ENSG000001	HOXB8	-2.1185241
ENSG000000	DCN	2.11845579
ENSG000002	AL359220.1	2.11668192
ENSG000001	CPZ	2.11349382
ENSG000001	TMPRSS2	-2.105955
ENSG000001	CTHRC1	2.0985844
ENSG000001	ADAM12	2.09492245
ENSG000001	MDFIC	2.0921297
ENSG000001	PCDH18	2.08884384
ENSG000000	ABCC9	2.08883494
ENSG000001	HOXB5	-2.0862379
ENSG000000	CHDH	-2.082894
ENSG000000	GRHL2	-2.0825277
ENSG000002	TRIM31	-2.0753583
ENSG000001	OLFML3	2.07502339
ENSG000000	BCS1L	-2.0699924
ENSG000001	DUSP7	2.06829642
ENSG000001	MNX1	-2.0681692
ENSG000002	CFI	2.06794984
ENSG000002	AC010503.4	-2.066242
ENSG000002	Metazoa_SRF	-2.0654099
ENSG000002	LINC01133	-2.0638474
ENSG000001	TJP3	-2.0638381
ENSG000001	LRG1	-2.0561147
ENSG000001	TMC5	-2.0496207
ENSG000001	GRASP	2.04825901
ENSG000001	CAVIN2	2.04445143
ENSG000001	ADGRL2	2.04185607
ENSG000001	IGIP	2.04035174
ENSG000001	TM4SF5	-2.032937
ENSG000001	GPR4	2.02614618
ENSG000002	C2orf72	-2.0235642
ENSG000001	HNF1A	-2.0217032
ENSG000001	CYP3A5	-2.0196008
ENSG000000	ATP2C2	-2.0193725
ENSG000001	AFAP1L1	2.01902945
ENSG000001	MST1	-2.0169282
ENSG000001	DTX3	2.01671556
ENSG000001	ADAMTS4	2.01491999
ENSG000001	SHH	-2.0132371
ENSG000001	BRIP1	-2.0122988
ENSG000001	KCNE4	2.01065693
ENSG000000	PLEKHG6	-2.0098157
ENSG000000	NGFR	2.00625839
ENSG000001	GRTP1	-2.0033983
ENSG000000	USH1C	-2.0017494

	*Target Identifier	Name
1	NM_005248.3	FGR
2	NM_000492.4	CFTR
3	NM_144617.3	HSPB6
4	NM_016429.4	COPZ2
5	NM_015982.4	YBX2
6	NM_153676.4	USH1C
7	NM_001291485.2	CEACAM7
8	NM_001384598.1	PLEKHG6
9	NM_203395.3	IYD
10	NM_032951.3	MLXIPL
11	NM_014228.5	SLC6A7
12	NM_001920.5	DCN
13	NM_001389466.1	DPEP1
14	NM_018397.5	CHDH
15	NM_000618.5	IGF1
16	NM_001003931.4	PARP3
17	NM_002773.5	PRSS8
18	NM_000218.3	KCNQ1
19	NM_203468.3	ENTPD2
20	NM_014861.4	ATP2C2
21	NM_002507.4	NGFR
22	NM_004809.5	STOML1
23	NM_002744.6	PRKCZ
24	NM_020297.4	ABCC9
25	NM_003561.3	PLA2G10
26	NM_004963.4	GUCY2C
27	NM_001079866.2	BCS1L
28	NM_006486.3	FBLN1
29	NM_004460.5	FAP
30	NM_024915.4	GRHL2
31	NM_001856.4	COL16A1
32	NM_014244.5	ADAMTS2
33	NM_177973.2	SULT2B1
34	NM_017893.4	SEMA4G
35	NM_021924.5	CDHR5
36	NM_002579.3	PALM
37	NM_006418.5	OLFM4
38	NM_024307.3	GDPD3
39	NM_031476.4	CRISPLD2
40	NM_001261841.2	TMC5
41	NM_001267560.2	TJP3
42	NM_000095.3	COMP
43	NM_000777.5	CYP3A5
44	NM_178176.4	MOGAT3
45	NM_003014.4	SFRP4
46	NM_000168.6	GLI3
47	NM_017680.5	ASPN
48	NM_001393.4	ECM2
49	NM_199168.4	CXCL12
50	NM_017763.6	RNF43
51	NM_002982.4	CCL2
52	NM_003006.4	SELPLG
53	NM_000900.5	MGP
54	NM_001385079.1	PDE10A
55	NM_002317.7	LOX
56	NM_004624.4	VIPR1
57	NM_138393.4	REEP6
58	NM_001039348.3	EFEMP1
59	NM_024758.5	AGMAT
60	NM_001366006.2	ADGRL2
61	NM_001130173.2	MYB
62	NM_001901.4	CCN2
63	NM_003239.5	TGFB3
64	NM_024016.4	HOXB8
65	NM_002147.4	HOXB5
66	NM_004417.4	DUSP1
67	NM_000474.4	TWIST1
68	NM_005086.5	SSPN
69	NM_002429.6	MMP19
70	NM_000493.4	COL10A1
71	NM_007115.4	TNFAIP6
72	NM_001024630.4	RUNX2
73	NM_022449.4	RAB17
74	NM_024636.4	STEAP4
75	NM_017436.7	A4GALT
76	NM_001299.6	CNN1
77	NM_005515.4	MNX1
78	NM_005110.4	GFPT2
79	NM_003734.4	AOC3
80	NM_032192.4	PPP1R1B
81	NM_001082971.2	DDC
82	NM_005518.4	HMGCS2
83	NM_002262.5	KLRD1
84	NM_002334.4	LRP4
85	NM_000775.4	CYP2J2
86	NM_000545.8	HNF1A
87	NM_001166345.3	MDFIC
88	NM_032043.3	BRIP1
89	NM_000035.4	ALDOB
90	NM_001388308.1	KIF12
91	NM_182757.4	RNF144B

92	NM_000104.4	CYP1B1
93	NM_001370299.1	AMIGO2
94	NM_002345.4	LUM
95	NM_006329.4	FBLN5
96	NM_002009.4	FGF7
97	NM_003839.4	TNFRSF11A
98	NM_001554.5	CCN1
99	NM_000396.4	CTSK
100	NM_001039362.2	ATP6V1C2
101	NM_002398.3	MEIS1
102	NM_001378074.1	BOC
103	NM_003013.3	SFRP2
104	NM_003999.3	OSMR
105	NM_005564.5	LCN2
106	NM_014317.5	PDSS1
107	NM_014576.4	A1CF
108	NM_001288973.2	ADAM12
109	NM_001040694.2	INCENP
110	NM_080671.4	KCNE4
111	NM_020675.4	SPC25
112	NM_000722.4	CACNA2D1
113	NM_004181.5	UCHL1
114	NM_001378183.1	PIEZO2
115	NM_152550.4	SH3RF2
116	NM_052924.3	RHPN1
117	NM_130386.3	COLEC12
118	NM_005099.6	ADAMTS4
119	NM_080860.4	RSPH1
120	NM_001185.4	AZGP1
121	NM_203314.3	BDH1
122	NM_001864.4	COX7A1
123	NM_181711.4	TAMALIN
124	NM_001761.3	CCNF
125	NM_002644.4	PIGR
126	NM_152386.4	SGPP2
127	NM_012134.3	LMOD1
128	NM_002181.4	IHH
129	NM_001443.3	FABP1
130	NM_020208.4	SLC6A20
131	NM_001947.4	DUSP7
132	NM_001130682.3	GUCY1A1
133	NM_000193.4	SHH
134	NM_138455.4	CTHRC1
135	NM_025098.4	MOGAT2
136	NM_002404.3	MFAP4
137	NM_001150.3	ANPEP
138	NM_005379.4	MYO1A
139	NM_022097.4	CHP2
140	NM_001288702.2	GGT6
141	NM_001988.4	EVPL
142	NM_206918.3	DEGS2
143	NM_004657.6	CAVIN2
144	NM_004560.4	ROR2
145	NM_001393586.1	MYO7B
146	NM_024017.5	HOXB9
147	NM_052972.3	LRG1
148	NM_024922.6	CES3
149	NM_199161.5	SAA1
150	NM_020998.4	MST1
151	NM_001532.3	SLC29A2
152	NM_000196.4	HSD11B2
153	NM_005282.3	GPR4
154	NM_178502.4	DTX3
155	NM_005301.5	GPR35
156	NM_153636.3	CPNE7
157	NM_017570.5	OPLAH
158	NM_001795.5	CDH5
159	NM_001144950.2	SSC5D
160	NM_020211.3	RGMA
161	NM_005708.5	GPC6
162	NM_005656.4	TMPRSS2
163	NM_003062.4	SLIT3
164	NM_001012302.3	ANO9
165	NM_023944.4	CYP4F12
166	NM_003247.5	THBS2
167	NM_031475.3	ESPN
168	NM_001377530.1	DMBT1
169	NM_002725.4	PRELP
170	NM_172167.3	NOXO1
171	NM_000668.6	ADH1B
172	NM_003480.4	MFAP5
173	NM_001056.4	SULT1C2
174	NM_004791.3	ITGBL1
175	NM_001167600.3	NEU4
176	NM_007028.5	TRIM31
177	NM_032451.2	SPIRE2
178	NM_000204.5	CFI
179	NM_152246.3	CPT1B
180	NM_001375484.1	CKMT1B
181	NM_003809.3	TNFSF12
182	NM_006873.4	STON1

SUPPLEMENTARY MATERIALS AND METHODS

Sample preparation and sequencing

RNA sequencing was performed on the same platform for all patient cohorts included in this work, whether or not they were treated with ICI. For the DNA analyses, all exome sequencing was performed with comparable qualitative parameters (e.g., ~50X depth for normal samples and ~200X depth for tumor samples). The exome profiles were produced by the Integragen platform. For the C2 cohort (targeted NGS panel, ICM platform), depth of coverage was likely similar, comprised between 50X and 300X. For the C1 cohort, genomic DNA isolated from formalin- fixed paraffin-embedded (FFPE) were captured using Twist Human Core Exome Enrichment System (Twist Bioscience) + IntegraGen Custom as previously described [1]. For the C2 cohort, hybridization probes and extension primers were designed using Roche's HyperDesign Tool for NGS Target Enrichment process. Sequence capture, enrichment and elution were performed according to manufacturer's instruction and protocols without modification except for library preparation performed with NEBNext® Ultra II kit (New England Biolabs®). DNA samples were then sequenced on an Illumina NovaSeq as Paired-end 100 reads. The generated reads were mapped to the reference genome hg38 (GRCh38).

Exome Analysis and Mutational load

Variant calling for the identification of SNVs (Single Nucleotide Variations) and small insertions/deletions (up to 20bp), was performed via the Broad Institute's GATK Haplotype Caller GVCF tool (GATK3.8.1) for constitutional DNA and via the Broad Institute's MuTect tool (2.0, --max_alt_alleles_in_normal_count=2; --max_alt_allele_in_normal_fraction=0.04) for somatic DNA. A two-sided Fisher's Exact Test is applied after MuTect2 variant calling to improve filtering of variants with strand bias. The tumor mutational burden (TMB) is calculated by dividing the number of somatic mutations by the number of bases having a depth greater than 10. The somatic mutations used for the mutational load were filtered as follows: Somatic score ≥ 3,

Mutated Allele Frequency in Tumor tissue ≥ 5%, Mutated Allele Count in Tumor tissue ≥ 3, Mutated Allele Frequency in Constitutional tissue < 4%.

MHC class-I neoepitopes prediction

Neoepitopes prediction was performed using *Ideation*@SiRIC pipeline which combines several software. First, HLA typing for MHC class-I genes was carried out using seq2HLA [2] software for all 26 normal-wes fastq files, with default parameters. Next, Somatic mutation filtered VCF files from Mutect2 were annotated by Variant Effect Predictor (Version 99) with default parameter, except for the using of 'Frameshift' and 'wild-type' plugins offer by pVACseq from pVACtools suite [3]. After annotation, the variant items that lead to peptide changes were extracted out for downstream analysis. vcf-expression-annotator from VAtools v5.0.1 were then used to add transcripts expression levels (using 3' RNA sequencing) for each variant. Annotated non-synonymous mutations, frameshift variants and sequencing-based information as well as HLA class-I gene typing results inferred by seq2HLA were fed into pVACseq for neoantigen prediction. For each pVACseq run, epitope prediction was done by both NetMHC [4] and NetMHCpan [5] algorithms packed in pVACseq toolkit, epitope length was set to 8–10 with default parameters used for all other settings. At last, we applied coverage and expression-based filters besides median binding affinity filtering criteria on the predicted neoepitopes. We filtered neoepitope with tumor DNA VAF <= 5%, along with TPM >=1 for transcript level expression. Afterward, we kept only neoepitopes with TSL (Transcript Support Level) equal to 1 and median affinity binding <=500. To calculate the number of neoepitopes per tumor, we sum up unique filtered mutants peptides sequences per tumor.

Feature selection and data pre-processing

To reduce our dataset (over 279 positions explored) to the most relevent positions, we decided to keep only the positions with a Cox regression *p*-value in Nipicol lower than 0.05 [6]. We also decided to only focus on variations in microsatellite regions. Finally, we have applied a filter to the maximum rate of missing data allowed in a position in Nipicol. To do so, we firstly calculated this value in other available WES cohorts of MSI CRC, i.e., the public cohort TCGA and two other large private cohorts

we have already sequenced and analyzed in the lab (data not shown). This allows us to exclude positions that are generally difficult to sequence. Secondly, we did the same on the Nipicol cohort to exclude the remaining mis-sequenced positions. We have chosen to allow a maximum of 5% of missing data per MS over the external WES or Nipicol. With those filters we selected 19 microsatellite variations of interest.

In order to train a MNB model on our DNA sequencing data, we had process missing sequencing data at certain locations for some patients. Indeed, MNB does not support missing data in its learning or prediction. As a result, the missing data must be imputed. We imputed missing data using by using a discrete uniform distribution drawing wild-type or mutated based on the mutation frequency of the microsatellite.

DNA signatures : mutation count and Multinomial Naives Bayes

To calculate normalized mutation count we firstly had to take into account the impact of the mutation on the ICI response. To do so, we inverted the status of the microsatellite mutation associated with a good response to ICI. As a results we obtained a matrix containing for each patient the genotype effect for each microsatellite (0 for beneficial and 1 for deleterious). Then, for each patient, we summed up the microsatellite status and divided it by the number of microsatellite sequenced.

For the MNB, we used a matrix containing the mutation status for each microsatellite in every Nipicol patient (1 for mutated, 0 for wild-type) as the input values and the iPFS status as the binary target values. We obtained a model that was able to predict the progression risk of a patient taking into account its sequencing on the 19 microsatellites investigated.

To validate our models, we calculated the mutation count and predicted the progression risk for each ImmunoMSI patients. Then we ran an univariate Cox regression model to investigate the association between the survival and those new signatures.

Transcriptome profile generation and analysis

Total RNA was extracted for every tumor sample using QIAGEN Allprep protocol (ref 10.2144/000113829). 150ng of total RNA was used to generate RNAseq sequencing library using Lexogen Quantseq 3' FWD kit and sequenced by the Institut du cerveau iGenseq plateform on a NovaSeq 6000 aiming for a minimum of 10 million reads. Raw RNAseq reads were mapped to the human genome (Ensembl GRCH38) and Ensembl's reference transcriptome using STAR. Gene counts were obtained using FeatureCount, normalized by an UpperQuartile procedure and logged on a base 2.

Gene-set definitions of pathways were taken from the Molecular Signature Database (MSigDB v7.5.1) as well as the BioPlanet pathways database (2019) which was downloaded from the EnrichR website. Pathway-level activity was inferred from gene expression levels using the GSVA method with a Gaussian kernel. Based on the ImmuneDeconv evaluation and implementation, five methods for tumor microenvironment quantification were used: XCell, EPIC, Cibersort, MCPcounter and Estimate. Multiple hypotheses testing correction using Benjamini-Hochberg's to control False Discovery Rate (FDR) was only applied to select significant events using an alpha 5% to reject H0.

Independent Component Analysis (ICA) was performed on the sample-wise centered gene expression values of the 5,000 genes with the highest average and variable (as measured by standard deviation) expression. The JADE (joint approximation diagonalization of Eigen-matrices) algorithm was applied to extract 10 components as previously described [7]. The ICA components were projected on other transcriptomic dataset by first selecting genes in common in the reference ICA (computed from the C1 cohort) and in the new transcriptomic dataset. The cross-product of the gene-weight inverted matrix was used as the projection of a new dataset, resulting in 10 scores (one per ICA component) for each new sample.

The intra-tumor proportion of the consensus molecular subtypes of colorectal cancer were estimated using the centroids of the original study [8] and the WISP deconvolution method (cit-bioinfo.github.io/WISP/).

1 Gnirke A, Melnikov A, Maguire J et al. Solution hybrid selection with ultra-long oligonucleotides for massively parallel targeted sequencing. Nat Biotechnol 2009; 27 (2): 182-189.

2 Boegel S, Lower M, Schafer M et al. HLA typing from RNA-Seq sequence reads. Genome Med 2012; 4 (12): 102.

3 Hundal J, Kiwala S, McMichael J et al. pVACtools: A Computational Toolkit to Identify and Visualize Cancer Neoantigens. Cancer Immunol Res 2020; 8 (3): 409-420.

4 Lundegaard C, Lamberth K, Harndahl M et al. NetMHC-3.0: accurate web accessible predictions of human, mouse and monkey MHC class I affinities for peptides of length 8-11. Nucleic Acids Res 2008; 36 (Web Server issue): W509-512.

5 Reynisson B, Alvarez B, Paul S et al. NetMHCpan-4.1 and NetMHCIIpan-4.0: improved predictions of MHC antigen presentation by concurrent motif deconvolution and integration of MS MHC eluted ligand data. Nucleic Acids Res 2020; 48 (W1): W449-W454.

6 Polsterl S, Conjeti S, Navab N et al. Survival analysis for high-dimensional, heterogeneous medical data: Exploring feature extraction as an alternative to feature selection. Artif Intell Med 2016; 72: 1-11.

7 Puleo F, Nicolle R, Blum Y et al. Stratification of Pancreatic Ductal Adenocarcinomas Based on Tumor and Microenvironment Features. Gastroenterology 2018; 155 (6): 1999-2013 e1993.

8 Guinney J, Dienstmann R, Wang X et al. The consensus molecular subtypes of colorectal cancer. Nat Med 2015; 21 (11): 1350-1356.

Supplementary Table S1: Patients description from C1 and C2 cohorts with corresponding clinical data

ECOG, Eastern Cooperative Oncology Group performance-status scores range from 0 to 5, with higher scores indicating greater disability. CR, complete response; PR, partial response; SD, stable disease; PD, progressive disease.

Supplementary Table S2: NIPICOL and ImmunoMSI cohorts with clinical data including survival data

Supplementary Table S3: List of the genes most contributing to the stromal signature

Supplementary Table S4: List of the genes (n=182 genes) in the reduced stromal signature

Supplementary Figure S1. Correlations between MSISensor, MSICare and other genomic instability indexes, analysis of their clinical relevance to predict ICI resistance in MSImCRC patients

Supplementary Figure S2. Progression free survival (iPFS) curve according to non-repetitive Gene variant status

Kaplan-Meier survival curves plotted for progression-free survival (iPFS) according to some Genes mutation status (Wild type are indicated in grey and mutated in dark-red).

Supplementary Figure S3: Predictive nature of this 19-plex identified DNA signature

Analysis based on the concomitant analysis of their somatic variations in tumor DNA as compared to matched normal DNA by simply calculating for each patient the mean count of all the mutations in those MS.

Supplementary Figure S4: Transcriptome analysis

A-B) Univariate analyses of the association between cell population quantification estimation or single-gene expression levels and the objective response to ICI as evaluated by iRECIST and iPFS in the two cohorts C1 (a) and C2 (b).

(C-H) Distribution of Cox's proportional hazard *p*-value measuring the association of tumor microenvironment signatures (c,f), Pathway's estimated activity (d,g) or single-gene expression levels (e,h) with progression-free survival in C1 and in either the entire C2 (c,d,e) or only in the subset of C2 in which patients received the same combination of ICI than in C1 (f,g,h). In the plots, *p*-values are signed so that association with increased risk (HR > 1) are positive and association with decreased risk (HR < 1) are negative.

Supplementary Figure S5. Testing association of pathway activity to objective response as evaluated by iRECIST and progression free survival by iRECIST (iPFS)

Univariate association of pathway activity estimated by GSVA in C1 NIPICOL cohort (left) and C2 ImmunoMSI cohort (right). Gene set defining pathways were taken Bioplanet collection by default, or Elsevier pathway collection and BIOCARTA when specified.

Supplementary Figure S6. Characterization of the four RNA components defined by ICA in C1 NIPICOL

Four RNA components defined by ICA were significantly associated with objective response defined by iRECIST. From left to right: Pathway enrichment (NES: normalized enrichment score), C1 iRECIST objective response, univariate association with iPFS in C1, association with objective response defined by iRECIST in C2 and univariate association with iPFS in C2. The boxes go from the upper to the lower quartiles, and the whiskers go from the minimum to the maximum value, the line in the box corresponds to the median (C1: n=41 ; C2: n = 70).

Supplementary Figure S7. RNA signatures

A) Correlation of the stromal signature, defined by ICA, with tumor cellularity estimated by exome sequencing.

B) Univariate association of the intra-tumoral proportion of CMS with progression-free survival by iRECIST.

Supplementary Figure S8. Quantification of Sirius Red staining in MSI mCRC samples with low or high stromal RNA signature

A) Box plot of the percentage of fibrosis assessed by automated morphometry and according to the stromal signature (high >0, low <0). The boxes go from the upper to the lower quartiles and the line in the box corresponds to the median.
B) Correlations between the percentage of fibrosis assessed by automated morphometry and the stromal signature.

Supplementary Figure S9: Multivariate analysis of both signatures in patients

A) Forest plot of the multivariate Cox regression with progression-free survival in cohort C2, representing hazard ratio (HR < 1 : beneficial, HR = 1 No effect, HR > 1 : deleterious) with its corresponding p.value. Included features are DNA signature (low to high risk), stromal RNA signature (low to high fribose score), BRAF, KRAS (wild-type vs mutated), and treatment type (mono vs. combo).
B) Heatmap representation, in C1 (n=23) and C2 (n=66), of the DNA and RNA models predictions in regard with the patients iPFS, iRECIST status and the treatment (combo-therapy or mono-therapy) (27).

Supplementary Figure S10: **Reduced RNA stromal signature**
A) Spearman correlation between the original transcriptome-wide component and the reduced signature.
B) Kaplan-Meier curves of iPFS using reduced RNA signature (n=182 genes) and the same cut-off as with the original signature in Nipicol (C1) and ImmunoMSI (C2).
C) Forestplot of the reduced RNA stromal signature and the DNA signature as well as the treatment type considering the continuous value (upper panel) or by discretizing the values (lower panel) of the signatures.
D) Kaplan-Meier estimates of iPFS as a function of the intensity combination of the reduced RNA signature and the DNA signature (n=66). High RNA and DNA signatures are shown in red. Low RNA and DNA signatures are shown in green. High RNA signature and weak DNA signature are shown in orange and low RNA signature and high DNA signature are shown in purple.